学位論文

Study on the roles of the trans-Golgi network and RAB11 family on endocytosis in plant cells

植物細胞のエンドサイトーシスにおけるトランスゴルジ網と RAB11 ファミリーの機能の研究

平成２４年１２月博士（理学）申請

東京大学大学院理学系研究科

生物科学専攻

崔　勝媛

Abstract

Environmental cues are perceived at the plasma membrane (PM), which evokes downstream signaling to induce the specific response. Cell surface proteins play critical roles in the perception of environmental stimuli at the PM and ensuing signal transduction. Intracellular localization of such proteins must be strictly regulated, which requires elaborate integration of exocytic and endocytic trafficking pathways. Subcellular localization of *Arabidopsis thaliana* FLAGELLIN SENSING 2 (FLS2), a receptor that recognizes bacterial flagellin, also depends on membrane trafficking. However, our understanding about the mechanisms involved is still limited. In this study, I visualized ligand-induced endocytosis of FLS2 using green fluorescent protein (GFP)-tagged FLS2. Upon treatment with the flg22 peptide, internalized FLS2-GFP from the PM was transported to a previously unknown compartment with an intermediate property of the trans-Golgi network (TGN) and the multivesicular endosome, which gradually discarded the characteristics of the TGN along the trafficking pathway. I further found that the endocytic processes of FLS2 involve RABA/RAB11 members at distinct steps; RABA4c and RABA6a function on transport of internalized FLS2 to and from the intermediate compartment, respectively. Moreover, I demonstrated that transport of *de novo*-synthesized FLS2 to the PM also involves a

distinct RABA/RAB11 member, RABA1b. My results demonstrate the complex regulatory system for properly localizing FLS2 and functional differentiation in RABA members in endo- and exocytosis.

Table of Contents

Acknowledgements

Completion of this doctoral thesis was possible with the support of several people. I would like to express my sincere gratitude to all of them. First of all, I am grateful to my adviser, Dr. A. Nakano, for his valuable guidance I received throughout the research work. I thank Dr. T. Ueda, for his support and consistent encouragement on the whole steps of the research. I also thank Dr. T. Uemura for his valuable suggestions and concise comments on the research work.

To perform this research, I thank Nam-Hai Chua (Rockefeller University) for providing the plasmid pMDC7 and S. Betsuyaku and M. Shimizu for their generous support in experiments using *N. benthamiana*, and S. Robatzek for providing the FLS2-GFP construct and fruitful discussions. This work was supported by Grants-in-Aid for Scientific Research and the Targeted Proteins Research Program (TPRP) from the Ministry of Education, Culture, Sports, Science and Technology of Japan (AN and TU), and JST, PRESTO (TU).

The thesis would not have come to a successful completion, without the scholarship I received from Ministry of Education, Culture, Sports, Science and Technology (MEXT) and Atsumi International Foundation (AISF).

The lab members have been very kind enough to extend their help at various phases of this research. I really thank all for their personal and scholarly interactions and suggestions of my research. I consider it as a great opportunity to do my doctoral program in this lab.

Finally I am very much indebted to my parents, sister and friends, who encouraged me at every stage of my personal and academic life. I owe it to my husband who supports me in every possible way to enable me to its completion.

Abbreviations

BOR1 REQUIRES HIGH BORON 1

BRI1 BRASSINOSTEROID INSENSITIVE 1

FLS2 FLAGELLIN SENSING 2

flg22 flagellin 22

MVEs multivesicular endosomes

PM plasma membrane

SNARE soluble N-ethyl-maleimide-sensitive factor attachment protein receptor

TGN trans-Golgi network

VHA-a1 VACUOLAR PROTON ATPASE A1

Chapter 1: Introduction

Eukaryotic cells recognize their environment mainly through proteins on the plasma membrane (PM), including receptors and sensors, which evoke intracellular signal transduction to respond to environmental cues. In animal cells, endocytosis plays critical roles in regulation of the amount of PM proteins responding to extracellular stimuli, transduction of signals from endosomes, and down regulation of the signal transduction (Sorkin and Von Zastrow, 2002; von Zastrow and Sorkin, 2007; Platta and Stenmark, 2011). Also in plants, there are several PM proteins whose localization is known to be regulated by endocytosis upon extracellular stimuli. For example, REQUIRES HIGH BORON 1 (BOR1), a boron efflux carrier on the PM, is endocytosed in response to changes in environmental boron concentration (Takano et al., 2002, 2005). The leucine-rich repeat (LRR) receptor serine/threonine kinase FLAGELLIN SENSING 2 (FLS2) is another example of localization regulated by endocytosis. FLS2 is the receptor for bacterial flagellin, and the *fls2* mutant is highly susceptible to infection by pathogenic bacteria (Zipfel et al., 2004). FLS2 recognizes 22 amino acids of a conserved domain in the N-terminus of flagellin (flg22 peptide; Felix et al., 1999), and FLS2 bound with flg22 is rapidly internalized from the PM into the cytoplasm and degraded probably in vacuoles (Robatzek et al., 2006) (Figure 1). Intriguingly, plants expressing $FLS2^{T867V}$, which has a mutation in a putative phosphorylation site, exhibit susceptibility to pathogenic *Pseudomonas syringae*, and flg22-triggered internalization of this mutant protein rarely occurs, indicating tight coupling of endocytosis of FLS2 and flagellin signaling (Robatzek et al., 2006). In the case of another LRR receptor kinase, BRASSINOSTEROID INSENSITIVE 1 (BRI1), its endocytosis is not induced by the ligand brassinosteroid, while brassinosteroid signaling is also regulated by

endocytosis of BRI1 (Geldner et al., 2007; Irani et al., 2012).

Thus, endocytosis and endocytic organelles play fundamental roles in a variety of plant functions, including responses to environmental cues and hormone signaling. However, our knowledge of the molecular mechanisms of endocytosis in plant cells is still limited. It is apparently insufficient to simply extend the knowledge obtained from yeast and animal systems to the plant system because the plant endocytic pathway seems to operate differently from these other organisms. The role of the *trans*-Golgi network (TGN) in endocytosis is a remarkable example. The TGN acts as the sorting platform for secreted and vacuolar/lysosomal proteins in eukaryotic cells. In addition to this function, the TGN in plant cells also acts as the early endosomes (Figure 2); a lipophilic tracer of endocytosis, FM4-64, stains the TGN bearing the TGN markers VHA-a1, SCAMP1, RABA2a, or RABA3 before this dye reaches the multivesicular endosomes (MVEs) marked by the conventional RAB5 ortholog ARA7/RABF2b (Dettmer et al., 2006; Lam et al., 2007; Chow et al., 2008). Immunoelectron microscopic analysis has also demonstrated that endocytosed BRI1 and BOR1 pass through the TGN and MVE (Viotti et al., 2010).

Regarding the molecular machineries of endocytosis, plants also seem to diverge from the animal system, as is evident when we compare organization of RAB GTPases between animals and plants. RAB GTPase is an evolutionarily conserved key player in membrane trafficking, which generally regulates the docking step of transport carriers to target organelles through the conformational change between GTP-bound active and GDP-bound inactive states. RAB GTPases are widely conserved in all eukaryotic lineages, which, however, seem to have been diversified in a way that is unique to each lineage. Molecular phylogenetic analyses have suggested that most land

plant RAB GTPases are classified into eight families, each of which exhibits high similarity respectively to animal RAB1, RAB2, RAB5, RAB6, RAB7, RAB8, RAB11, and RAB18 (Rutherford and Moore, 2002; Vernoud et al., 2003). The plant lacks clear homologs of the well-characterized animal endocytic RABs, RAB4 and RAB9, which also suggests that the regulatory mechanism of the plant endocytic pathway differs from the animal system. On the other hand, RAB5 and RAB11 members, which act in the endocytic pathway in animal cells, have been diversified in a unique way in plants. The plant RAB5/RABF family consists of two distinct subgroups, the plant-unique ARA6 group and the conventional RAB5 group. How these subgroups functionally differentiated has been unclear, but recent studies indicate that ARA6 is involved in trafficking from endosomes to the PM whereas conventional RAB5 acts in the vacuolar trafficking pathway (Sohn et al., 2003; Bolte et al., 2004; Kotzer et al., 2004; Ebine et al., 2011). Another outstanding characteristic of the plant RAB GTPase is the notable variety of RAB11 homologs (referred to as RABA in *Arabidopsis thaliana*). A total of 26 members of the 57 RAB GTPases in *A. thaliana* are classified into the RAB11 group; RABA, which is further divided into six subgroups (RABA1–RABA6) (Figure 3). RAB11 regulates the endocytic pathway in animal cells; animal RAB11 resides on recycling endosomes and regulates recycling of endocytosed proteins to the PM (Ullrich, 1996; Ren et al., 1998). On the other hand, yeast homologs of RAB11, Ypt3 members, are proposed to be required for multiple steps of the exocytic pathway including *intra*-Golgi transport and transport vesicle formation at the TGN (Benli et al., 1996; Jedd et al., 1997; Cheng et al., 2002). Some members of the plant RABA/RAB11 group also take part in several different exocytic events unique to plants. Substantial roles in tip growth of pollen tubes and root hairs have been demonstrated in *Nicotiana tabacum* and *A.*

thaliana (de Graaf et al., 2005; Preuss et al., 2004; Szumlanski and Nielsen, 2009), and expression of dominant negative RABA2a inhibits cytokinesis of root tip cells in *A. thaliana* (Chow et al., 2008). RABA1b has been also reported to regulate trafficking between the TGN and PM (Feraru et al., 2012; Asaoka et al., 2012). It remains unclear, however, whether each RABA group regulates a distinctive trafficking pathway and if any of the subgroups are involved in endocytic trafficking.

In this study, I at first visualized and characterized the endocytic route of FLS2, whose internalization was induced by flg22 treatment, in leaf epidermal cells of *Nicotiana benthamiana*. By comparing localization of internalized FLS2 with TGN and MVE markers, I identified a novel transient compartment with a hybrid property between the TGN and MVE, which appears to be an intermediate organelle mediating endocytosis of FLS2. I then attempted to explore functions of RABA subgroups in the intracellular transport of FLS2 to find distinct functions of different subgroups of RABA. My results indicate discrete functional differentiation among RABA subgroups in endocytic and exocytic pathways.

Chapter 2: Results

flg22-dependent internalization of FLS2 in *Nicotiana benthamiana* leaf epidermal cells

In this study, I applied the transient expression system in *Nicotiana benthamiana* leaf epidermal cells by infiltration of agrobacterium, which has been successfully used to observe intracellular trafficking of fluorescent protein-tagged proteins and simultaneous expression of multiple proteins (Goodin, Chakrabarty, Yelton, et al., 2007; Goodin, Chakrabarty, Banerjee, et al., 2007; Tardif et al., 2007; Martin and Kopperud, 2009; Wang et al., 2011). At first, I confirmed localization of green fluorescent protein (GFP)-tagged FLS2 on the PM in untreated *N. benthamiana* cells (Figure 4A), as reported in *A. thaliana* leaf epidermal cells (Robatzek et al., 2006). Then I examined whether flg22-dependent internalization of FLS2-GFP is also observed in this system. Upon treatment with flg22, dot-like structures with FLS2-GFP appeared in the cytoplasm 90 min and 120 min after flg22 application (Figures 4B and 4C). On the other hand, treatment with $flg22^{A.tum}$, the inactive peptide derived from *Agrobacterium tumefaciens* flagellin (Felix et al., 1999), did not result in accumulation of FLS2-GFP at the cytoplasmic organelles (Figure 4D), indicating that flg22 specifically triggers endocytosis of FLS2 in this system. To examine earlier events of endocytosis of FLS2 in this system, I then observed the behavior of FLS2-GFP by a total internal reflection fluorescence microscopy (TIRFM)-related technique called variable-angle epifluorescence microscopy (VAFM) or variable incidence angle fluorescence microscopy (VIAFM) that enables selective visualization of sample surface regions (Fujimoto et al., 2007; Konopka and Bednarek, 2008). FLS2 signals were concentrated on the PM during 40 min after applying flg22 (Figures 4E to 4G), and clear punctuate signals probably reflecting concentrated or internalized FLS2 were observed in 60 min on or near the PM

(Figure 4H).

FLS2 is transported to unknown compartments with a hybrid nature between the TGN and MVE

To investigate which organelles are involved in endocytosis of FLS2, I co-expressed FLS2-GFP with mRFP-SYP61 or VHA-a1-mRFP, markers of the TGN, or TagRFP-ARA7 or TagRFP-VAMP727, markers for the MVE, because these organelles are known to act as endocytic compartments in plant cells (Ueda et al., 2001; Uemura et al., 2004; Takano et al., 2005; Dettmer et al., 2006; Lam et al., 2007; Viotti et al., 2010). From 90 min to 120 min after flg22 treatment, FLS2-GFP was observed overlapping or associated with mRFP-SYP61 (Figures 5A and 5B). On the other hand, FLS2-GFP was not observed near the SYP61 compartments after 210 min (Figure 5C). For quantitative analysis of this observation, I extracted the dot-like signals of FLS2-GFP and mRFP-SYP61 and measured the distance from the center of a FLS2-GFP–positive dot to that of the nearest mRFP-SYP61 signal using a macro run on the Metamorph software that our lab previously developed (Ito et al., 2011). The results were categorized into three groups by distances: (a) colocalized (≤0.24 μm: below the resolution limit of the objective lens used in this study); (b) associated (≤1 μm); and (c) independent (>1 μm). I compared results between two groups of samples; one was observed from 80 to 140 min after flg22 treatment (an early endocytic stage), and the other was observed from 140 to 200 min after flg22 application (a late endocytic stage). In the early stage, about 27.6% ± 6.4% and 39.6% ± 6.5% of FLS2-positive compartments were colocalized and associated with SYP61-positive dots, respectively (Figure 5R). On the other hand, ratios of colocalized and associated groups were significantly decreased to 5.6% ± 3.9% and

19.3% ± 6.6%, respectively, in the late endocytic stage (n = 3 experiments, $P < 0.01$, Student's t test) (Figure 5R). These results suggested that internalized FLS2 upon flg22 application transiently localizes at SYP61-positive compartments in the early stage. Intriguingly, an experiment using another TGN marker VHA-a1 yielded a different result. When VHA-a1 and FLS2 were coexpressed and treated with flg22, I did not observe colocalization of these proteins in any time points after the flg22 treatment (Figures 5D to 5F). The quantitative analysis also supported this observation; only 1.0% ± 0.9% and 1.0% ± 1.7% of FLS2-positive compartments were categorized to colocalization in early and late stages, respectively (Figure 5S), in my colocalization analysis. For further clarification of this result, I compared subcellular localization of CFP-SYP61 and VHA-a1-mRFP in cells expressing FLS2-GFP, whose endocytosis was induced by flg22 treatment. SYP61- and VHA-a1-postivie dots were mostly overlapped, however, I found that the SYP61-positive compartments carrying FLS2-GFP did not harbor VHA-a1-mRFP (Figures 5M to 5P). I also confirmed that SYP61 tagged with CFP or mRFP exhibited the same localization pattern (Figure 5Q). These results clearly indicated that the compartment bearing SYP61 and FLS2 observed in this study harbors a distinct characteristic from the TGN in cells where endocytosis of FLS2 is not induced.

I next examined whether TagRFP-tagged ARA7 and VAMP727, a MVE-localizing RAB GTPase and R-SNARE, respectively, were colocalized with FLS2. These endosomal proteins were localized on FLS2-positive puncta observed in both early and late stages (Figures 5G to 5L, 5T and 5U).

To investigate the relationship between SYP61- and ARA7-positive compartments in flg22-induced endocytosis of FLS2, I then expressed FLS2-GFP, mRFP-SYP61, and

TagRFP-ARA7 in the same cell and compared their subcellular localization after treatment with flg22. At the earlier stage (100 min after the treatment), both SYP61 and ARA7 were colocalized on the same FLS2-positive compartments (Figure 6A). On the other hand, after 140 min, most SYP61 localization did not overlap with FLS2 or ARA7 but occurred instead at the membrane domains in close proximity to (or associated with) the FLS2- and ARA7-positive domains (Figure 6B). After 200 min, I did not see colocalization or association of SYP61 with FLS2, while FLS2 still exhibited good colocalization with ARA7 at this time point (Figure 6C). These results indicated an unknown endosomal compartment involved in flg22-triggered endocytosis of FLS2, which seemed to harbor an intermediate property between the TGN and MVE. Of interest, the colocalization of SYP61 and ARA7 was observed only at compartments carrying endocytosed FLS2-GFP. In *A. thaliana* plants grown under normal laboratory conditions, our laboratory have noted no significant colocalization between the MVE and TGN proteins thus far (Ebine et al., 2008, 2011). Thus, such intermediate compartments might exist only when endocytosis is highly activated.

To verify this possibility, I compared localization of SYP61 and ARA7 after flg22 treatment between two samples: leaf epidermal cells expressing FLS2-GFP, mRFP-SYP61, and TagRFP-ARA7, and cells expressing mRFP-SYP61 and TagRFP-ARA7 but not FLS2-GFP. As observed above, 4.6 % ± 2.0% of mRFP-SYP61-positive compartments bore TagRFP-ARA7 in FLS2-expressing cells at 100 min after application of flg22 (Figures 6D and 6E); this is significantly higher than the ratio (1.1 % ± 0.5 %) of mRFP-SYP61 compartments with TagRFP-ARA7 in cells not expressing FLS2 after treatment with flg22 ($n = 3$ experiments, $P < 0.05$, Student's t test; Figures 6F and 6G, and Table 1). These results suggested that the intermediate

compartment identified in this study is a transient endosomal structure that is induced when endocytosis is highly activated. Under my experimental conditions, about 20% of SYP61-positive compartments were classified as “associated” with ARA7-positive compartments, which indicated that two compartments were not overlapped but in close proximity (0.24 μm < distance between two compartments ≤1 μm), regardless of combinations of coexpressed proteins and time points (Table 1).

Effects of mutant RABA on endocytosis of FLS2

As described above, I found that previously unknown compartments with intermediate properties between the TGN and MVE are involved in ligand-induced endocytosis of FLS2. To identify molecular machineries that control the trafficking pathway around the novel compartment, I focused my interest on the RABA family because some RABA members have been reported to act in membrane trafficking around the TGN (Preuss et al., 2004; de Graaf et al., 2005; Chow et al., 2008), although involvement of this family in endocytosis remains totally unexplored. Because of the extreme expansion of RABA members in *A. thaliana* (Table 2), it is not practical at present to test their involvement in endocytosis of FLS2 using genetic mutants. Thus I took advantage of the transient expression system in *N. benthamiana* leaf epidermal cells, which allowed us to monitor the effect of a dominant-negative mutant of each RABA subgroups whose expression was conditionally induced in cells expressing FLS2-GFP and organelle markers. I created a nucleotide-free mutant of each member of the six subgroups of RABA (RABA1b, RABA2c, RABA3, RABA4c, RABA5c, and RABA6a) by replacing invariable asparagine in the conserved GNKXD sequence with isoleucine (hereafter called the NI mutant), because these mutants have been successfully used as dominant-negative

forms for functional analyses of RABA members in plants (Cheung et al., 2002; Chow et al., 2008; Bottanelli et al., 2011). The expression of the NI mutants was controlled by an estradiol-inducible promoter (Zuo et al., 2000) to avoid undesirable effects of the mutant expression on transport of newly synthesized FLS2 to the PM. I examined the effects of these mutants on endocytic transport of FLS2-GFP, comparing its subcellular localization with SYP61 and/or ARA7. For induction of mutant expression, 10 μM estradiol was infiltrated into *N. benthamiana* leaves and incubated for 2–3 h, and then samples were treated with flg22. This condition is enough for accumulation of the mutant RABA members, as indicated by bright fluorescence from Venus fused to the mutant RABA members (Figure 7). I examined the effects of expression of wild-type and NI mutants for all six RABA subgroups, three of which (RABA2c, RABA3, and RABA5c) had no substantial effect on endocytic transport of FLS2-GFP; mutants of RABA3 and RABA5c did not exert significant effects on endocytosis of FLS2 ($P > 0.05$, Student's *t* test), and the mutant of RABA2c had only a marginal effect on colocalization with SYP61 at the later stage; $P = 0.0493$, Student's *t* test; Figures 8 to 10). However, expression of NI mutants of the other three RABA subgroups resulted in remarkable alteration in endocytic trafficking of FLS2-GFP.

RABA6a and RABA4c act in distinct steps of FLS2 endocytosis

In RABA6a^{N126I}-expressing cells, I found that FLS2 colocalized well with SYP61 even at the late stage, at which FLS2 was observed on membrane compartments independent of SYP61-domains in wild-type RABA6a-expressing cells (Figure 11A). Quantification analysis further indicated that expression of RABA6a^{N126I} increased colocalization of FLS2 with SYP61. I found that 41.2% ± 4.0% and 15.4 ± 3.5% of FLS2-positive

compartments in early (80 to 140 min) and late (140 to 200 min) stages, respectively, also bore SYP61 in RABA6a^{N126I}-expressing cells, which was significantly higher than that observed in wild-type RABA6a-expressing samples (21.6% ± 5.9% in the early stage and 5.2% ± 2.6% in the late stage, n = 3 experiments, $P < 0.05$, Student's *t* test; Figure 11B). This result appeared to indicate that RABA6a acts in trafficking of FLS2 from SYP61-positive compartments. I then examined whether ARA7 also occurs on the FLS2-positive compartments in RABA6a^{N126I}-expressing cells. I coexpressed TagRFP-ARA7 with FLS2-GFP and mutant or wild-type RABA6a to find that ARA7 also localized on FLS2-positive compartments in both cases (Figure 12). These results strongly suggested that RABA6a^{N126I} did not impair formation of the hybrid compartment bearing SYP61 and ARA7 but did cause delay in transport or transition from the intermediate endosome to the SYP61-free late endosomal compartment, which resulted in increased colocalization of FLS2 and SYP61 in NI mutant-expressing cells.

Intriguingly, RABA4c^{N128I} conferred an apparently opposite effect from RABA6a^{N126I}. In cells expressing the RABA4c^{N128I} mutant, the extent of colocalization between FLS2 and SYP61 in the early stage was significantly reduced (5.8% ± 3.9%) compared with the result from coexpression of wild-type RABA4c (26.7% ± 9.6%, $n = 3$ experiments, $P < 0.05$, Student's *t* test; Figures 13A and 13B). This result appeared to indicate that internalized FLS2 was not transported to the SYP61 compartments in mutant-expressing cells. However, I found that ARA7 did colocalize with FLS2 in RABA4c^{N128I}-expressing cells (Figure 14). Thus, there might be an alternative direct trafficking pathway from the PM to ARA7-positive MVEs without transit through SYP61-positive compartments.

These results clearly indicated that two distinct RABA subgroup members,

RABA6a and RABA4c, regulate different steps in the endocytic pathway of FLS2. Furthermore, the specific effects of these RABA members also demonstrated that the inhibitory effects I observed in these experiments resulted from inhibition of the specific function of each RABA member in *N. benthamiana*, rather than reflecting the effect of titration of general RAB regulators such as RAB guanine nucleotide dissociation inhibitor. This notion was also supported by the results of coexpression of wild-type RABA members with NI mutants. I coexpressed mRFP-tagged wild-type RABA members with Venus-RABA4c^{N128I} or Venus-RABA6a^{N126I} for suppression activities for transport defects of FLS2 in tobacco cells expressing FLS2-GFP and CFP-SYP61. The inhibitory effects of NI mutants were specifically rescued by coexpression of their wild-type versions but not by the other RABA members, which again indicated specific inhibition of the distinct trafficking event by each mutant RABA as the cases for other plant RAB GTPases (Figures 11C and 13C, Batoko et al., 2000; Kotzer et al., 2004; Pinheiro et al., 2009). I then examined order of functions of two RABA members RABA4c and RABA6a in endocytic trafficking of FLS2 by double infiltration of their NI mutants. Simultaneous expression of RABA4c^{N128I} and RABA6a^{N126I} caused the same trafficking defect as RABA4c^{N128I} (Figure. 15). This result strongly suggested that RABA4c acts in the earlier step in endocytic trafficking of FLS2 than RABA6a.

RABA1b functions in the secretory pathway

The NI mutant of RABA1b (RABA1b^{N126I}) exerted the other interesting effect. When expressed with this mutant, distribution of mRFP-SYP61 and internalized FLS2-GFP was dramatically changed. mRFP-SYP61, which presented clear dot-shaped signals in wild-type RABA1b-expressing cells, was scattered to tiny dots throughout the

cytoplasm (Figure 16). Regarding FLS2-GFP, for which flg22 treatment induced endocytosis, I observed no dot-like signals in the mutant-expressing cells, but only smear signals that largely overlapped with mRFP-SYP61 (Figure 16). These results indicated that RABA1b^{N126I} did not block the internalization of FLS2 from the PM but that the morphology of compartments with SYP61 to which FLS2 was transported was severely affected.

These findings additionally suggested that expression of mutant RABA1b resulted in alteration of the morphology of the TGN. Because the TGN also plays fundamental roles in the secretory pathway, I then examined the effects of NI mutants of RABA1b and other RABA subgroups on the steady-state localization of FLS2-GFP at the PM. For this purpose, chimeric genes comprising a 35S promoter, mutant cDNA for each RABA member, and a 35S terminator were introduced with FLS2-GFP into *N. benthamiana* cells. Among mutants of the six RABA members I examined, only RABA1b^{N126I} caused substantial alteration in FLS2 distribution. In the RABA1b^{N126I}-expressing cells, FLS2 was mainly observed as scattered tiny dots throughout the cytoplasm, and weak localization to the PM was also visible (Figure 17A). Moreover, constitutive expression of RABA1b^{N126I} affected distribution of mRFP-SYP61; mRFP-SYP61 was also dispersed throughout the cytoplasm as observed in the induced-expression experiment (Figure 17B). These results indicated that transport of newly synthesized FLS2 to the PM was disturbed by defective trafficking around the SYP61-positive TGN in the mutant-expressing cells.

I also tested an inhibitory effect of RABA1b^{N126I} on transport of the other PM protein BOR1, a boron efflux carrier whose localization is regulated by external boron concentration (Takano et al., 2002, 2005). Steady state localization of BOR1 was slightly

different from that of FLS2; BOR1-GFP signal was observed on punctate organelles in addition to the PM, probably reflecting its constitutive internalization (Takano et al., 2005, Figure 18A). Coexpression of RABA1b^{N126I} also resulted in alteration of this localization pattern; BOR1 predominantly localized on scattered small dots in the cytoplasm and slight PM localization was also detected in cells expressing RABA1b^{N126I} (Figure 18B). This result again suggested that RABA1b acts in the secretory pathway. On the other hand, the NI mutants of RABA4c and RABA6a had no visible effect on presentation of FLS2-GFP and BOR1-GFP on the PM (Figures 17A, 18C and 18D). In a similar manner, NI mutants of RABA2c, RABA3, and RABA5c caused no substantial change in the PM localization of FLS2 (Figure 17A). The inhibitory effect of RABA1b^{N126I} in secretory trafficking of FLS2 was attributable to specific inhibition of the RABA1 function, because estradiol-induced coexpression of wild-type RABA1b, but not RABA4c or RABA6a, restored the PM localization of FLS2-GFP (Figure 17C). These results again support the specific and distinct functions of RABA subgroups in plant cells.

Distinct subcellular localizations of RABA1b, RABA4c, and RABA6a

It is interesting to ask whether three RABA members with different functions, RABA1b, RABA4c, and RABA6a, reside on different subcellular compartments or on the same organelle. I thus compared directly the localization of these proteins using combinations of different fluorescent proteins. Expression of fluorescent protein-tagged RABA members was induced by incubation with 10 μM estradiol for 1 h. RABA1b, RABA4c, and RABA6a localized at various sizes of dot-like structures (Figure 19A). These RABA members exhibited good colocalization on comparatively large compartments; however,

they did not overlap at small vesicular structures (Figure 19A). This different localization is not due to the difference in fused fluorescent proteins, because the RABA member tagged with different fluorescent proteins localized to the same compartments (Figure 19B).

In *A. thaliana* root epidermal cells, comparatively large compartments bearing RABA1b partly overlap with the TGN marked by SYP43 or VHA-a1 (Asaoka et al., 2012). Thus I then examined whether RABA members are also localized on the TGN in my experimental system. When coexpressed in FLS2-GFP expressing *N. benthamiana* leaf epidermal cells, Venus-tagged RABA members and mRFP-SYP61 frequently colocalized on larger particles, while mRFP-SYP61 did not target to RABA-positive smaller vesicles (Figure 19C). The colocalization between SYP61 and RABA1b was not affected by RABA4c^{N128I} and RABA6a^{N126I}, which exerted inhibitory effects on endocytic transport of FLS2 (Figure 19D and 19E). These results indicated that three RABA members localize on different compartments with overlap on the TGN, which is consistent with their different functions in transport of FLS2.

Chapter 3: Discussion

Internalized FLS2 is transported to intermediate compartments between the TGN and MVE

Endocytic transport of the flagellin receptor, FLS2, is tightly coupled with the plant defence response, thus it is of great interest and importance to understand the regulatory mechanism of this event (Robatzek et al., 2006). Recently, it has been shown that FLS2 internalized into cells in a ligand-induced manner passed through the distinct encodytic pathway from constitutively recycling FLS2. This report also indicated that conventional RAB5 is responsible for endocytosis of FLS2 (Beck et al., 2012). However, the identity of endosomal compartments mediating endocytic traffic of this receptor and molecular details of its mechanisms are remained largely unknown. In this study, I showed that internalized FLS2 passed through a compartment with a hybrid nature between the TGN and MVE and that localized both mRFP-SYP61 and TagRFP-ARA7 (Figure 20). The plant TGN is also recognized as an early endosome (EE) because an internalized lipophilic dye, FM4-64, stains the TGN earlier than the Rab5-positive MVEs (Dettmer et al., 2006; Lam et al., 2007; Chow et al., 2008). Consistent with these findings, Viotti et al. (2010) demonstrated by immunoelectron microscopy that the endocytosed cargo proteins BOR1 and BRI1 reach the TGN. Direct maturation from the TGN to MVE has also been proposed recently (Bottanelli et al., 2011; Scheuring et al., 2011), suggesting the sequential action of the TGN and MVE along the endocytic pathway. On the other hand, recent studies have indicated that plants also harbor a clathrin-independent mechanism of endocytosis (Li et al., 2012). Thus, the endocytic route could vary depending on each cargo, which would not be distinguishable by monitoring bulk membrane flow using FM dyes. What is now needed

is to monitor protein cargos to obtain robust and specific information.

To investigate the function of the TGN and MVE in ligand-triggered endocytosis of FLS2 and to examine which Rab GTPases are involved, I used the *N. benthamiana* transient expression system, which allowed us time-sequential and multi-color observation of endocytosed FLS2 and other trafficking components in living cells. In this system, I found that induction of endocytosis of FLS2 led to formation of a novel compartment that harbored both SYP61, a TGN-resident SNARE protein, and ARA7, the MVE-resident Rab GTPase, suggesting a nature of this intermediate compartment between the TGN and MVE. Interestingly, VHA-a1, another well characterized TGN protein, was not recruited to this hybrid compartment. Both SYP61 and VHA-a1 are shown to colocalize with SYP43, a SNARE protein residing on the TGN in *A. thaliana* root epidermal cells (Uemura et al., 2012). Thus my results could further indicate the unique character of the intermediate compartment; this compartment harbors a limited set of TGN proteins in addition to endosomal RAB5 GTPase. Because quantitative analyses in previous studies have shown that the known TGN markers were not colocalized completely (Dettmer et al., 2006; Chow et al., 2008; Boutté et al., 2010; Gendre et al., 2011), it would be also possible that a specific population of the TGN (or a specific membrane domain around the TGN) serves for flg22-triggered endocytic transport of FLS2. It would be an interesting future project to study how endocytic trafficking and remodeling of the TGN are integrated in plant cells.

Another important finding is that SYP61 appeared to segregate to distinct membrane domains from ARA7 and FLS2 and was gradually removed from the hybrid organelle, while FLS2 exhibited good colocalization with ARA7 even after a long incubation. This result suggests that the TGN components are gradually eliminated from the hybrid

compartment, leading to maturation to an MVE with a fully late endosomal nature. In agreement, endosomal sorting complex required for transport (ESCRT) components are gradually recruited to the TGN to lead maturation of the TGN to the MVE, and colocalization of SYP61 and ARA7 is also observed when the function of the TGN is hampered by concanamycin A or the function of the ESCRT complex is inhibited (Scheuring et al., 2011). Thus, my results, together with the findings by Scheuring et al., might suggest that maturation of the TGN to the MVE is at least partly responsible for ligand-induced endocytic trafficking of FLS2 to the vacuole.

Curiously, I did not observe a compartment harboring FLS2 and SYP61 without ARA7. This result raises two possibilities. The first is that internalized FLS2 is transported to the SYP61-positive but ARA7-negative TGN first, which, however, cannot be observed because of too-rapid maturation kinetics. Another possibility is that internalized FLS2 is transported directly to the hybrid endosomes bearing both SYP61 and ARA7. Although I have not detected colocalization of ARA7 and TGN markers at the steady state in my experimental system, another group reported that ARA7 is also detected at the TGN (Stierhof and El Kasmi, 2010). Thus, a small number of the hybrid organelles could exist in plant cells, with a population that might increase under specific conditions that require enhanced endocytosis. In a consistent manner, a recent study on FLS2 trafficking in *A. thaliana* also suggested that some population of ARA7-positive compartments could act as early endosomes (Beck et al., 2012). Regardless, further studies of this hybrid compartment are needed to reveal its nature and function. Whether other endocytic cargos also pass through this intermediate compartment and whether this hybrid compartment is observed when endocytosis is activated in other plants including *A. thaliana* would be interesting questions to address.

RABA/RAB11 groups have distinct functions in membrane trafficking around the TGN

I succeeded in finding RABA members whose respective dominant-negative mutants affect different steps of endocytosis of FLS2. RABA6a^{N126I} affected the maturation step from the hybrid endosomes to the LE/MVE; FLS2 retained localization on the hybrid endosomes with both SYP61 and ARA7 in RABA6a^{N126I}-expressing cells even after a long incubation, suggesting delay in the maturation process. In the animal system, early-to-late maturation of endosomes is associated with replacement of Rab GTPases, which is referred to as "Rab conversion." Rab5 on the early endosomes in animal cells is gradually replaced by Rab7, which is responsible for late endosomal trafficking mediated by effector complexes of these Rab GTPases, CORVET and HOPS (Rink et al., 2005). Considering the subcellular localization of RABA members around the TGN (Preuss et al., 2004; de Graaf et al., 2005; Chow et al., 2008), my results may indicate that plants also employ a similar molecular mechanism in endosomal maturation, which is associated with Rab conversion from RABA6a to ARA7.

On the other hand, coexpression of RABA4c^{N128I} resulted in a significant decrease in the endosome population with both SYP61 and FLS2, while internalization of FLS2 was not markedly affected. This result appears to indicate that FLS2 does not reach the TGN. Curiously, however, I found that ARA7 resided on the FLS2-positive compartment also in RABA4c^{N128I}-expressing cells. This observation might be explained by accelerated maturation from the hybrid compartment to the late endosome; however, that would not be likely because a dominant-negative Rab GTPase generally inhibits or delays trafficking events, which should also be the case for RABA4c^{N128I}. Thus, my finding may indicate an alternative trafficking pathway that mediates transport from

the PM to the ARA7-positive endosome directly when the early endocytic pathway to the TGN/EE is compromised. It would be also possible that the effects of RABA6a^{N126I} and RABA4c^{N128I} on colocalization of FLS2 and SYP61 represent altered distribution of SYP61; these mutant RABA members could affect transport of SYP61 to or from ARA7- and FLS2-positive endosomes. However, this situation would not be so likely, because the localization pattern of SYP61 and RABA1b was not affected by coexpression of RABA6a^{N126I} and RABA4c^{N128I}.

Another interesting finding is that RABA1b, a member of the largest subgroup of the six RABA subgroups, is involved in delivery of newly synthesized FLS2 and BOR1 to the PM. Coexpression of RABA1b^{N126I} resulted in dispersed localization of SYP61, which also indicates that this RABA member is responsible for maintenance of TGN distribution. On the other hand, RABA1b^{N126I} did not seem to affect internalization of FLS2 to the SYP61-positive compartment, as shown by relocalization to a dispersed pattern similar to that of SYP61 in RABA1b^{N126I}-expressing cells after flg22 treatment. I did not see any effects on FLS2 and SYP61 distribution for equivalent mutants of other members including RABA4c^{N128I} and RABA6a^{N126I} in both estradiol-induced and 35S promoter-driven constitutive expression. These results strongly suggest that the RABA1 group specifically acts in the secretory pathway but not in the endocytic pathway, which is also required for maintenance of TGN morphology. The RABA1b function in the secretory pathway is also suggested in *A. thaliana* plants (Asaoka et al., 2012)

Functional diversification of plant RABA members

My data clearly indicate that different RABA members have distinct functions in

intracellular trafficking of FLS2 (Figure 20). In a consistent manner, three members identified in this study as being involved, RABA1b, RABA4c, and RABA6a, exhibited distinct subcellular localization, supporting that these members act at different membrane domains around the TGN. Recent comparative genomics indicates that extreme expansion of Rab11 homologs is one of the most remarkable characteristics in organization of plant Rab GTPases. The reason for the expansion of plant Rab11 homologs and how their molecular functions are differentiated have been unclear, but my results indicate that the functions of RABA/Rab11 members are diversified from each other. Another important finding is that plant RABA/Rab11 is involved in both secretory and endocytic pathways. The functional diversity together with their important roles in plant-unique physiological events (Preuss et al., 2004; de Graaf et al., 2005; Chow et al., 2008; Szumlanski and Nielsen, 2009) indicate that expansion of this family could play pivotal roles in increased complexity of membrane trafficking pathways in plant cells, which are recruited to plant-unique physiological events during plant evolution. The next interesting question is how the RABA/Rab11 members encoded by a paralogous set of genes acquired diverse functions in membrane trafficking. Further functional analyses of this group, as well as identification and characterization of upstream regulators and downstream effectors, would be needed to answer this question.

Material and methods

Transient expression in *N. benthamiana* and flg22 treatment

I used 3–5-week-old *N. benthamiana* plants for agro-infiltration. Expression vectors were introduced into *A. tumefaciens* strain GV3101::pMP90. A single colony of the transformants was cultured in 5 mL YEB medium (5 g beef extract, 1 g yeast extract, 5 g sucrose, and 0.49 g $MgSO_4 \cdot 7H_2O$ dissolved in 1 L water) supplemented with 10 μg/mL rifampicin at 30°C overnight. The bacteria were collected and resuspended in infiltration buffer (10 mM MES, 10 mM $MgCl_2$, 0.15 mM acetosyringone, pH 5.5) at 0.02 (FLS2-GFP) or 0.1 (other constructs) OD_{600}. The agrobacteria carrying p19 was resuspended together with all samples (Voinnet et al., 2003). The resuspended agrobacteria were infiltrated to leaves of *N. benthamiana* with gentle pressure using syringes without needles. For coexpression of proteins, bacterial strains with different constructs were mixed before inoculation. Samples were observed within 48 h after infiltration. For induction of endocytosis of FLS2, 100 μM of flg22 peptide was infiltrated to leaves expressing FLS2-GFP. For estradiol-dependent induction of gene expression, ß-estradiol (10 μM) was applied for 1–3 h before treatment with flg22.

Plasmid construction

The plasmid containing pFLS2:FLS2-GFP was described previously (Robatzek et al., 2006). For mRFP-SYP61, VHA-a1-mRFP, TagRFP-ARA7, and TagRFP-VAMP727 constructs, PCR-amplified cDNA fragments Were cloned into pGWB1 containing the 35S promoter (Nakagawa et al., 2007). For RABA members (*RABA1b*, *RABA2c*, *RABA3*, *RABA4c*, *RABA5c*, and *RABA6a*), cDNA fragments were amplified by PCR using the following primers: RABA1b, 5'-CACCATGGCAGGGTACAGA-3' and

5’-TCAATTTGAGCAGCACCCGA-3’; RABA2c, 5’-CACCATGACGCATAGAGTAGATCA-3’ and 5’-GGCCGGATCCTTAAGAAGAGCAACATGCTC-3’; RABA3, 5’-CACCATGAACGAAGAGATGAGCG-3’ and 5’-TCAACACGAGCACGAAGCTTGT-3’; RABA4c, 5’-CACCATGTCAAAATTTCAGAGCAATTTCAATCAG-3’ and 5’-CTATGATGTTCCACAACAACCTTTTCCTTTAG-3’; RABA5c, 5’-CACCATGTCAGACGACGACGAGA-3’ and 5’-TTACCTCGAACAGCAAGAGAATGTC-3’; and RABA6a, 5’-CACCATGGCAGAAGATACGT-3’ and 5’-GTCGGAATCAAATCTGATCTCC-3’. Mutations Were introduced by PCR-based site-directed mutagenesis using the following primers: RABA1b, 5’-GGTTGGTatcAAATCTGATCTC-3’ and 5’-CAGATTTGATACCAACCAGCAT-3’; RABA2c, 5’-TCGGATTTGATCCCAGCCATCATG-3’ and 5’-ATGGCTGGGATCAAATCCGATCTGAACCAC-3’; RABA3, 5’-GCTTTGATTCCGACGAGCAT-3’ and 5’-GTCGGAATCAAAGCCGATCT-3’; RABA4c, 5’-GTGTCCCGAGATCAGTTTTGATTCCTATTAGC-3’ and 5’-TAGGAATCAAAACTGATCTCGGGACACTTC-3’; RABA5c, 5’-CACATTTGATCCCAATAAGCATTTTTGCT-3’ and 5’-TTGGGATCAAATGTGATCTCGAGAGC-3’; and RABA6a, 5’-CAGATTTGATTCCGACGAGG-3’ and 5’-GTCGGAATCAAATCTGATCTCC-3’. Amplified wild-type and mutant cDNA fragments were conjugated with cDNA for fluorescent proteins and cloned into pMDC7 (Curtis and Grossniklaus, 2003) for estradiol-inducible expression. For constitutive expression, cDNA fragments of RABA were introduced into pB7WGY2 and pH7WGR2 containing YFP and RFP, respectively

(Karimi et al., 2002).

Confocal laser scanning microscopy

For single-color imaging, GFP was excited by a diode-pumped solid-state laser (Cobolt Blues, Cobowet) at 473 nm and observed under a microscope (BX51, Olympus) equipped with a confocal scanner unit (CSU10, Yokogawa Electric) and a cooled CCD camera (ORCA-AG, Hamamatsu Photonics). Images were processed with IPLab software (BD Biosciences) and Photoshop CS5 (Adobe). Multi-color observation was performed using an LSM710 or LSM780 confocal microscope (Carl Zeiss) with the oil immersion lens (X63, NA = 1.40). Spectral unmixing (if necessary) and processing of obtained images were carried out using ZEN 2008 or ZEN 2011 software (Carl Zeiss). For dual-color imaging, GFP and Venus were excited at 488 nm, and the emission was collected between 501 and 545 nm. mRFP and Tag RFP Were exited at 561 nm, and the emission was collected between 570 and 615 nm. For three-color imaging, samples expressing fluorescent proteins (combinations of three of four XFPs: GFP, Venus, mRFP, and TagRFP) were excited at 488 and 561 nm and the emission was collected between 484 and 640 nm. For three- or four-color imaging using CFP, samples were excited at 405, 488, and 561 nm and the emission was collected between 411 and 633 nm. The colocalization analysis was performed as described previously (Ito et al., 2011) with Metamorph software (Molecular Devices).

Variable incidence angle fluorescence microscopy

The leaves from infiltrated *N. benthamiana* were placed on slide glass (76 × 26mm, Matsunami), covered with a 0.12–0.17-mm-thick coverslip (24 × 60mm, Matsunami),

and epidermal cells were observed under a fluorescence microscope (Nikon Eclipse TE2000-E and a CFI Apo TIRF ×100 H/1.49 numerical aperture objective) equipped with a Nikon TIRF2 system. GFP was simultaneously excited with 488nm laser. All images were acquired with an Andor iXonEM EMCCD camera; each frame was exposed for 100 ms. The acquired images were prepared and analyzed with Photoshop CS5 (Adobe Systems) and NIS-Elements software (Nikon).

Accession Numbers

The Arabidopsis Genome Initiative locus identifiers for the genes mentioned in this article are At5g46330 (*FLS2*), At1g28490 (*SYP61*), At2g28520 (*VHA-a1*), At4g19640 (*ARA7*), At3G54300 (*VAMP727*), At1g16920 (*RABA1b*), At3g46830 (*RABA2c*), At1g01200 (*RABA3*), At5g47960 (*RABA4c*), At2g43130 (*RABA5c*), and At1g73640 (*RABA6a*).

Figures

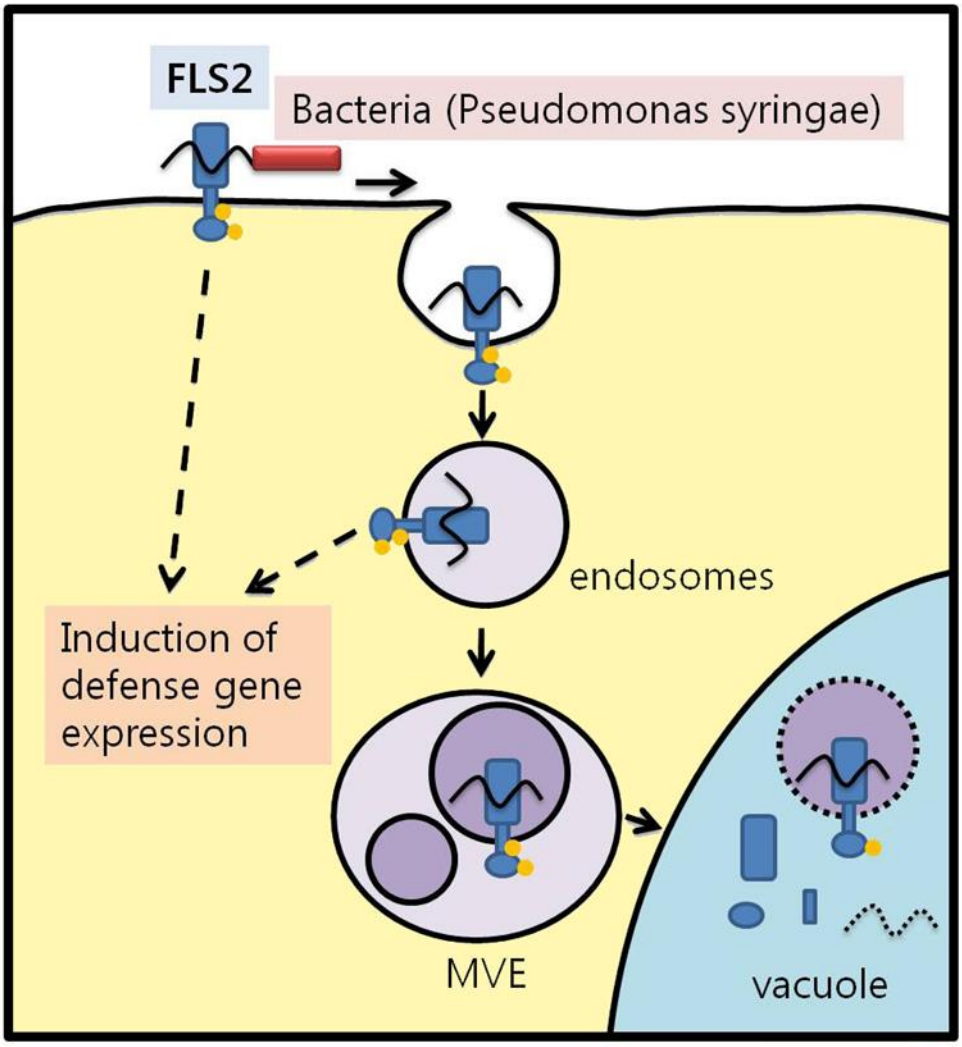

Figure 1. FLS2 is a receptor kinase which recognizes flagellin.
Depending on the binding of flg22, FLS2 enters endocytic pathway and induce of defence gene expression.

.

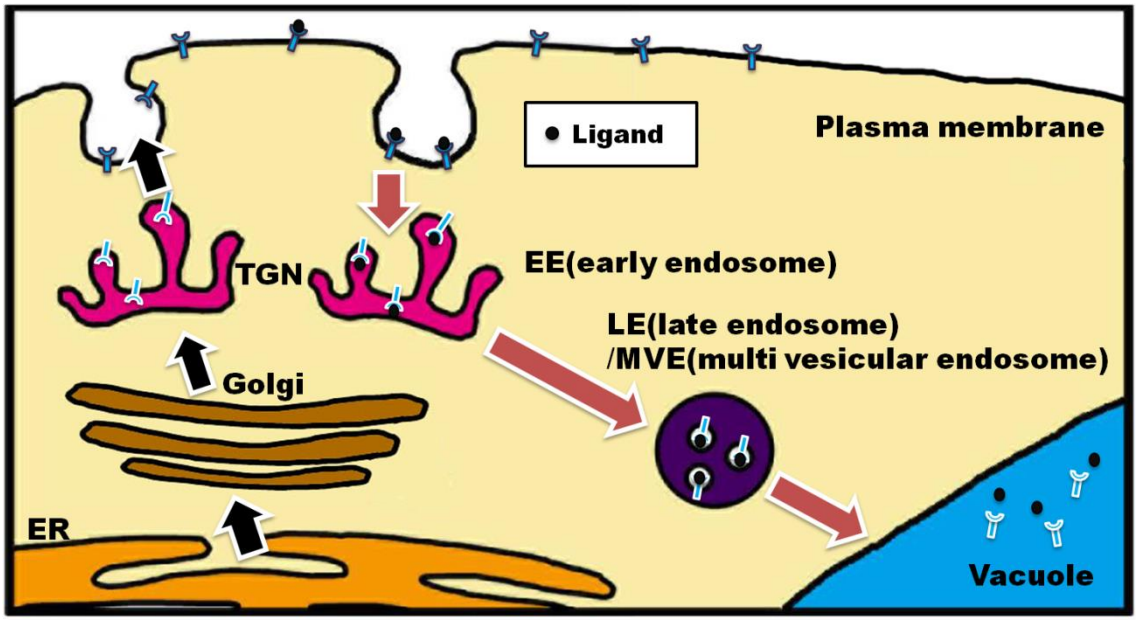

Figure 2. The TGN functions on exo- and endocytosis in plant cells.

Black and red arrows indicate exocytic and endocytic pathway, respectively.

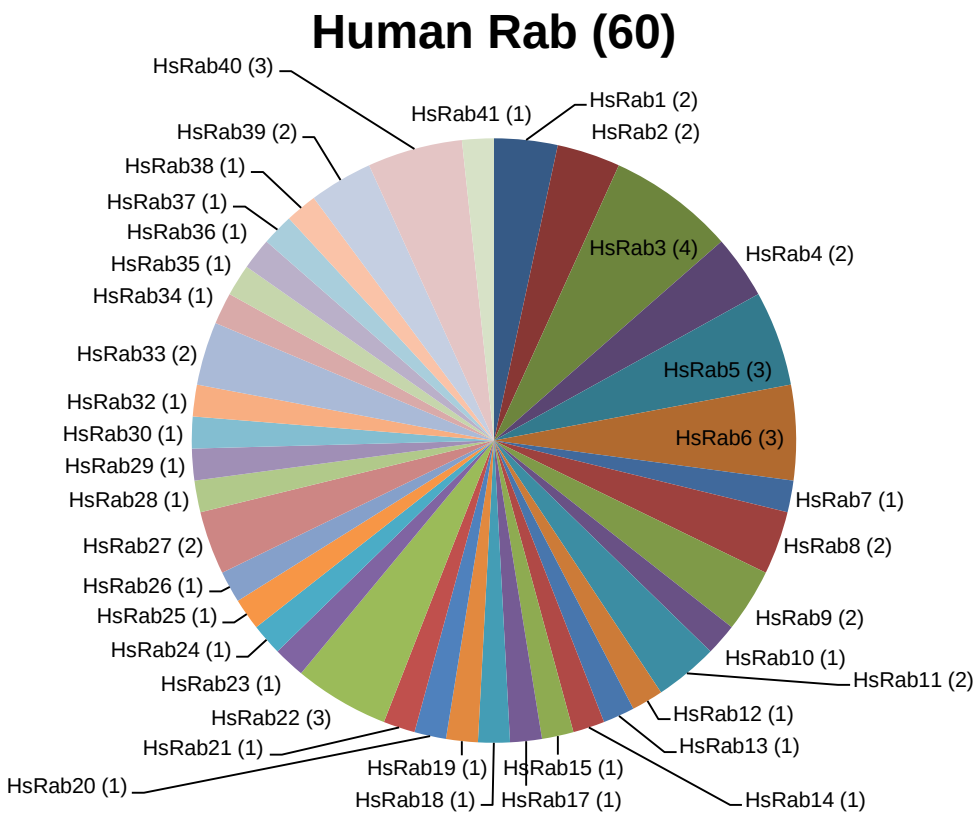
Human Rab (60)
HsRab40 (3)
HsRab41 (1)
HsRab1 (2)
HsRab2 (2)
HsRab39 (2)
HsRab38 (1)
HsRab37 (1)
HsRab36 (1)
HsRab35 (1)
HsRab34 (1)
HsRab33 (2)
HsRab32 (1)
HsRab30 (1)
HsRab29 (1)
HsRab28 (1)
HsRab27 (2)
HsRab26 (1)
HsRab25 (1)
HsRab24 (1)
HsRab23 (1)
HsRab22 (3)
HsRab21 (1)
HsRab20 (1)
HsRab19 (1)
HsRab18 (1)
HsRab15 (1)
HsRab17 (1)
HsRab14 (1)
HsRab12 (1)
HsRab13 (1)
HsRab10 (1)
HsRab11 (2)
HsRab9 (2)
HsRab8 (2)
HsRab7 (1)
HsRab6 (3)
HsRab5 (3)
HsRab4 (2)
HsRab3 (4)

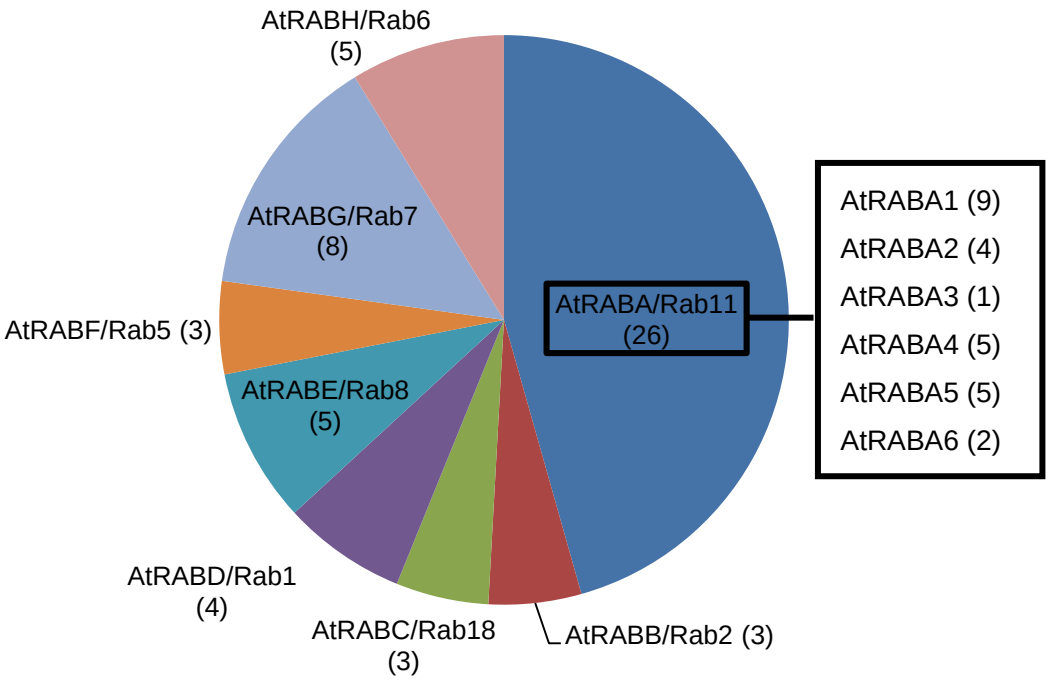
Arabidopsis RAB (57)
AtRABH/Rab6 (5)
AtRABG/Rab7 (8)
AtRABF/Rab5 (3)
AtRABE/Rab8 (5)
AtRABD/Rab1 (4)
AtRABC/Rab18 (3)
AtRABB/Rab2 (3)
AtRABA/Rab11 (26)
AtRABA1 (9)
AtRABA2 (4)
AtRABA3 (1)
AtRABA4 (5)
AtRABA5 (5)
AtRABA6 (2)

Figure 3. A comparison of the classification of RAB proteins in Human and Arabidopsis
The number in bracket indicates the number of members. The text box of RABAs indicates the subgroups.

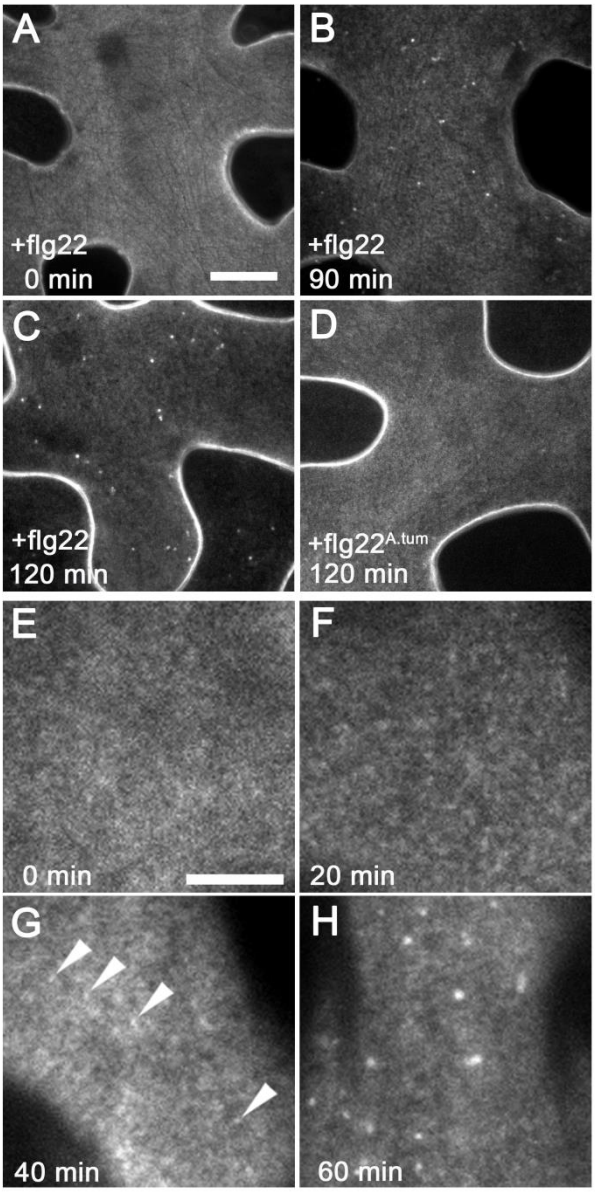

Figure 4. Endocytosis of FLS2-GFP in leaf epidermal cells of *N. benthamiana*.

(**A**) to (**D**) Max-intensity projection images are presented, each of which was reconstructed with a series of confocal Z-stack images taken at 0.5-μm intervals.

(**A**) FLS2-GFP localizes on the plasma membrane (PM) without any treatment. Bar = 10 μm. (**B**) FLS2-GFP is internalized into the cytoplasmic punctate compartments within 90 min of treatment with flg22. (**C**) Punctate compartments observed at 120 min after flg22 treatment. (**D**) Endocytosis of FLS2-GFP is not induced by flg22$^{A.tum}$ even after 120 min. (**E**) to (**H**) Variable incidence angle fluorescence microscopy of FLS2 in close proximity to the plasma membrane in 0 min (**E**), 20 min (**F**), 40 min (**G**), and 60 min (**H**) after flg22 treatment. Arrowheads indicate focal accumulation of FLS2 on the PM.

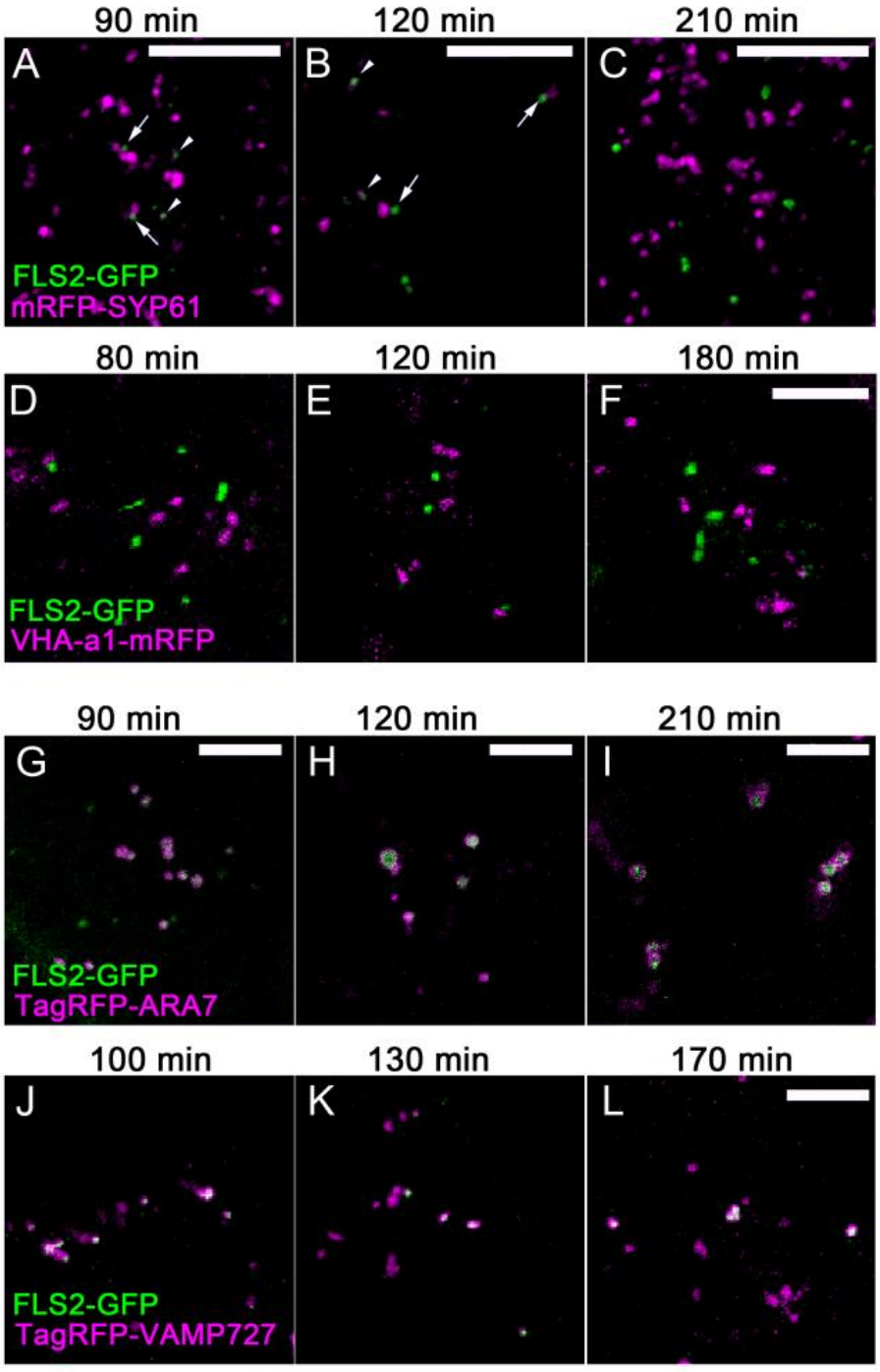
90 min
120 min
210 min
A
B
C
FLS2-GFP
mRFP-SYP61
80 min
120 min
180 min
D
E
F
FLS2-GFP
VHA-a1-mRFP
90 min
120 min
210 min
G
H
I
FLS2-GFP
TagRFP-ARA7
100 min
130 min
170 min
J
K
L
FLS2-GFP
TagRFP-VAMP727

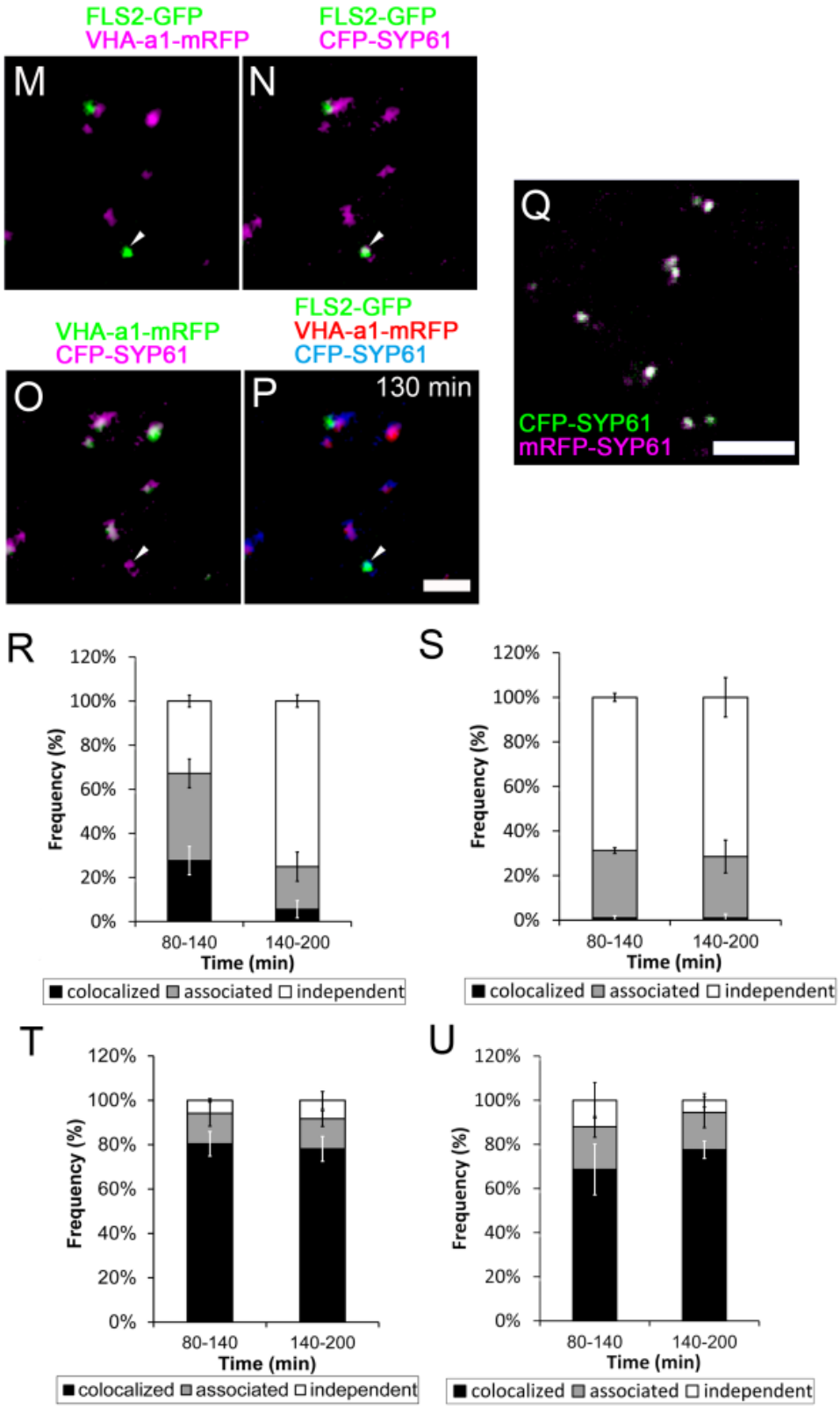

Figure 5. FLS2 is transported via SYP61- and ARA7-positive endosomal compartments.

(A) to (C) Time-course observation of FLS2-GFP endocytosis in mRFP-SYP61–expressing cells. Internalized FLS2-GFP colocalizes with mRFP-SYP61 at 90 min after flg22 treatment (A). After 120 min, FLS2-GFP is frequently observed associated with SYP61-positive compartments (B), but such colocalization and association are not observed after 210 min (C). Bars = 5 µm. Arrows and arrowheads indicate “associated” and “colocalized” compartments, respectively.

(D) to (F) VHA-a1-mRFP is not overlapped with FLS2-GFP. Bars = 5 µm.

(G) to (I) FLS2-GFP colocalizes with TagRFP-ARA7 at any time point. Bars = 5 µm.

(J) to (L) FLS2-GFP colocalizes with TagRFP-VAMP727 at any time point. Bars = 5 µm.

(M) to (P) Cells expressing FLS2-GFP, VHA-a1-mRFP, and CFP-SYP61 observed after 130 min of flg22 treatments. Bar = 5µm

(Q) CFP- and mRFP-tagged SYP61 completely overlapped when expressed in the same cell. Bar = 5µm

(R) to (U) Stacked bar graphs representing results of quantification of colocalization between FLS2-GFP and mRFP-SYP61 (R), FLS2-GFP and VHA-a1-mRFP (S), FLS2-GFP and TagRFP-ARA7 (T), or FLS2-GFP and TagRFP-VAMP727 (U). Data were collected from three independent experiments, 189 and 195 (FLS2-GFP and mRFP-SYP61), 209 and 186 (FLS2-GFP and VHA-a1-mRFP), 259 and 278 (FLS2-GFP and TagRFP-ARA7) or 178 and 158 (FLS2-GFP and TagRFP-VAMP727) FLS2-positive dots in total were observed in early (80–140) and late (140–200) stages, respectively. Error bars indicate the SD values.

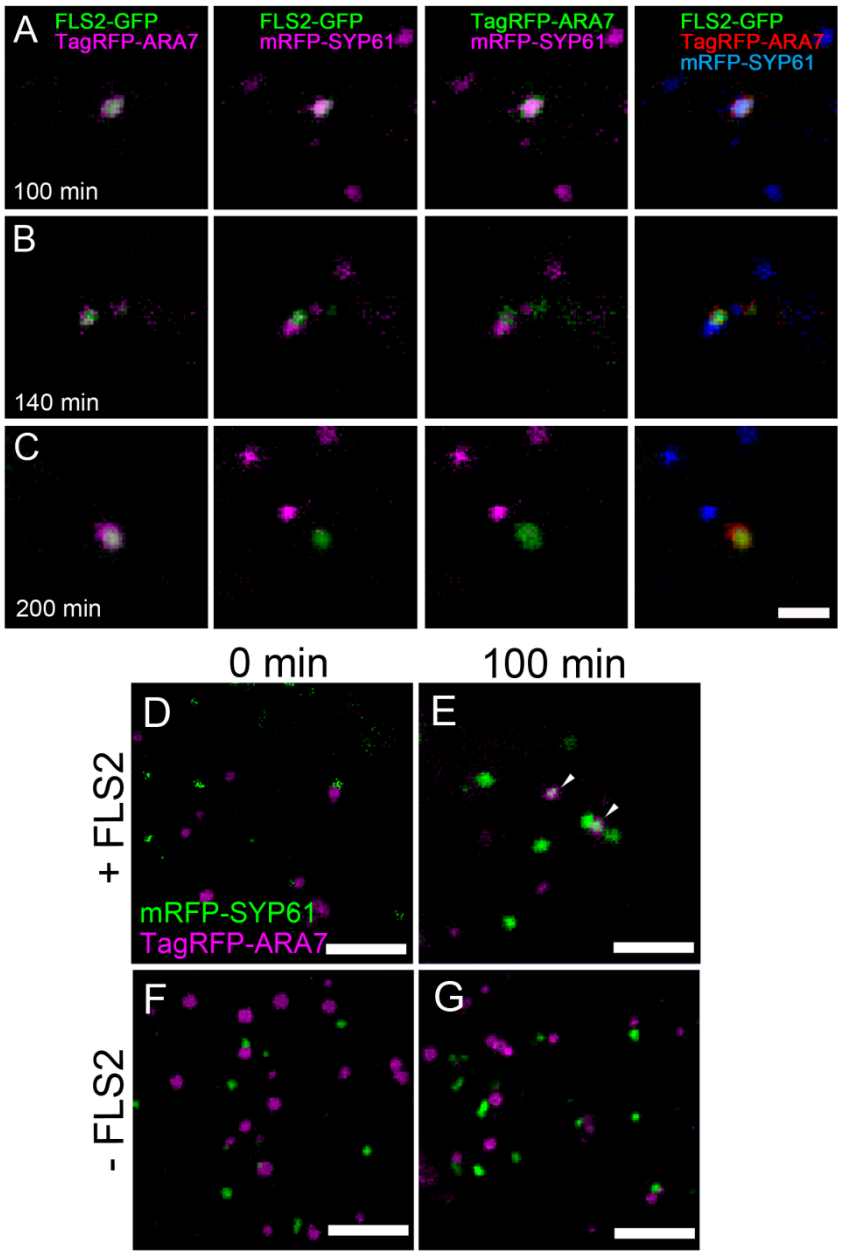

Figure 6. Hybrid nature of endosomal compartment involved in early FLS2 endocytosis.
(**A**) to (**C**) Cells expressing FLS2-GFP, mRFP-SYP61, and TagRFP-ARA7 observed after 100 min (A), 140 min (B), and 200 min (C) of flg22 treatment. Bar = 2 μm.
(**D**) to (**G**) The hybrid compartment is observed only when endocytosis of FLS2-GFP is induced. Cells expressing mRFP-SYP61 and TagRFP-ARA7 with FLS2-GFP ([D] and [E]) or without FLS2-GFP ([F] and [G]) were observed at 0 min or 100 min after flg22 treatment. Arrowheads indicate compartments bearing both mRFP-SYP61 and TagRFP-ARA7. Bars = 5 μm.

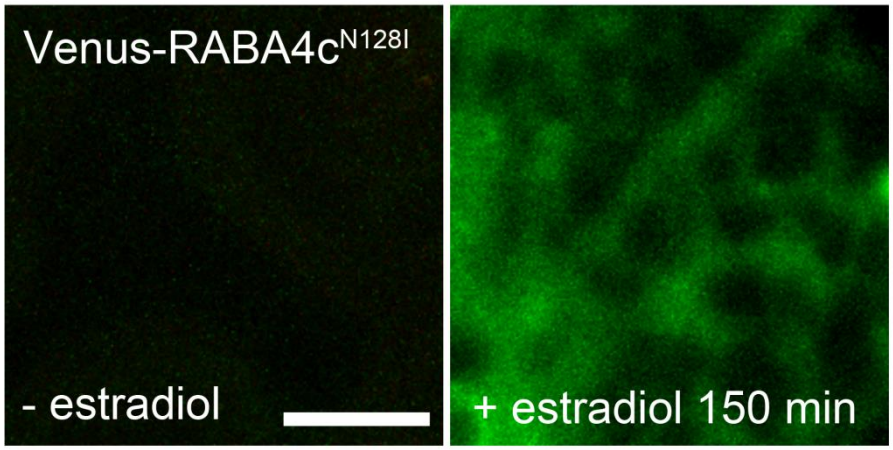

Figure 7. Estradiol treatment employed in this study efficiently induced gene expression.

Expression of Venus-tagged RABA4c subcloned into pMDC7 and introduced into *N. benthamiana* leaf epidermal cells was induced by estradiol treatment at 10 μM in 150 min.

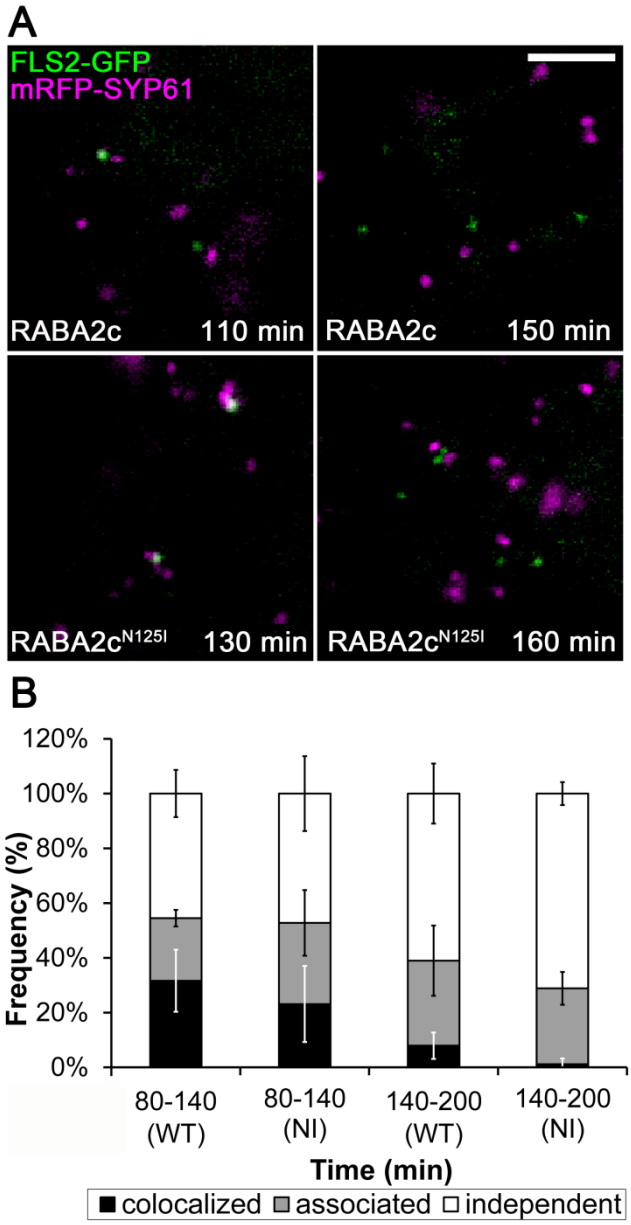

Figure 8. The NI mutant of RABA2c does not affect trafficking kinetics of FLS2-GFP.

(**A**) Cells expressing FLS2-GFP and mRFP-SYP61 with wild-type RABA2c (upper panels) or RABA2c^{N125I} (lower panels) were observed at indicated times after flg22 treatment. Expression of RABA2c and RABA2c^{N125I} was induced by estradiol treatment. Bar = 5 μm.

(**B**) Stacked bar graphs indicating results of quantitative analyses of colocalization between FLS2-GFP and mRFP-SYP61. WT, wild-type RABA2c-expressing cells; NI, RABA2c^{N125I}-expressing cells. Data were collected from three independent experiments, and 218 and 96 (WT) or 238 and 132 (NI) FLS2-positive dots in total were observed in early (80–140) and late (140–200) stages, respectively. Error bars indicate SD values.

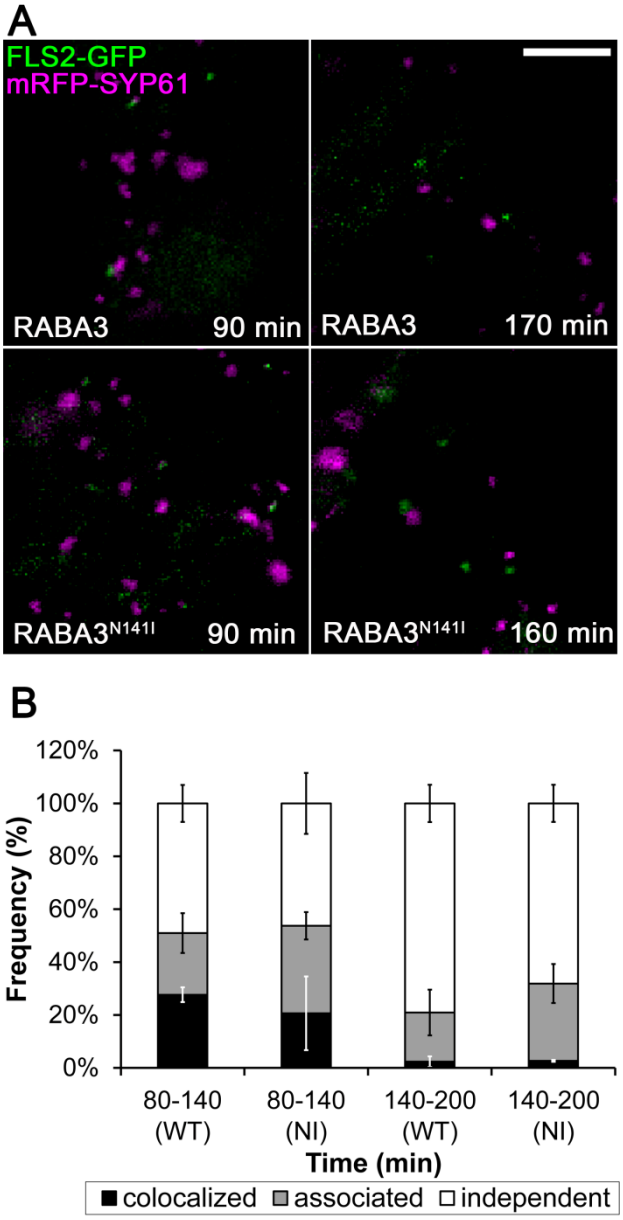

Figure 9. The NI mutant of RABA3 does not affect trafficking kinetics of FLS2-GFP.
(**A**) Cells expressing FLS2-GFP and mRFP-SYP61 with wild-type RABA3 (upper panels) or RABA3^{N141I} (lower panels) were observed at indicated times after flg22 treatment. Expression of RABA3 and RABA3^{N141I} was induced by estradiol treatment. Bar = 5 µm. (**B**) Stacked bar graphs indicating results of quantitative analyses of colocalization between FLS2-GFP and mRFP-SYP61. WT, wild-type RABA3-expressing cells; NI, RABA3^{N141I}-expressing cells. Data were collected from three independent experiments, and 174 and 120 (WT) or 162 and 114 (NI) FLS2-positive dots in total were observed in early (80–140) and late (140–200) stages, respectively. Error bars indicate SD values.

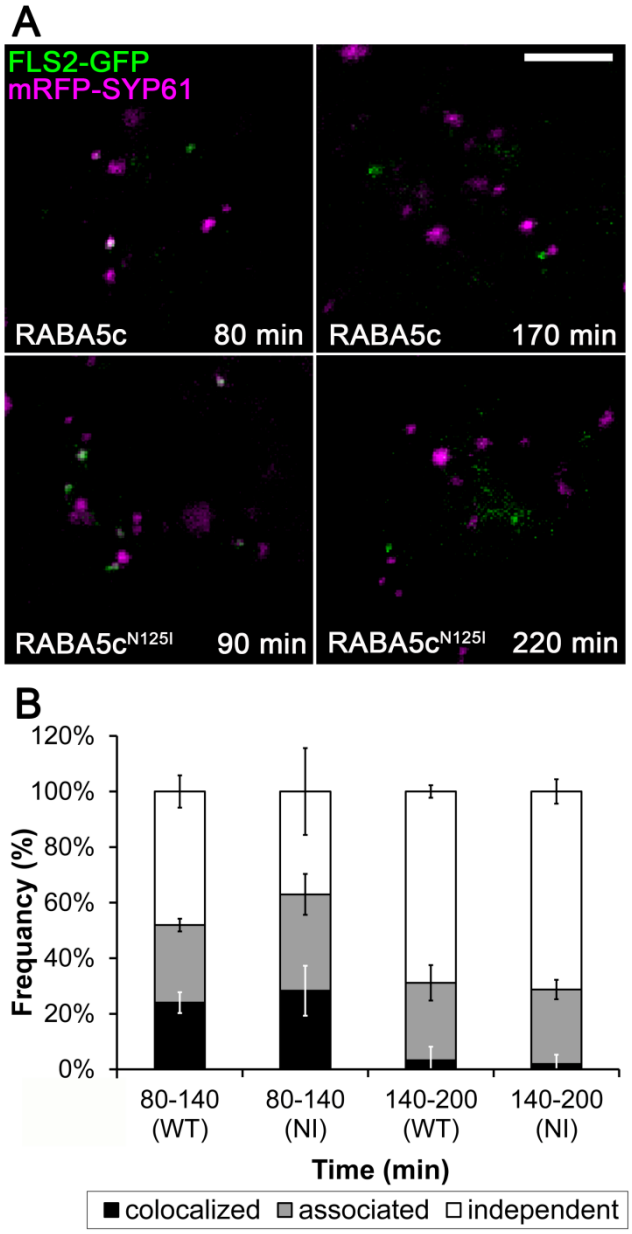

Figure 10. The NI mutant of RABA5c does not affect trafficking kinetics of FLS2-GFP.

(A) Cells expressing FLS2-GFP and mRFP-SYP61 with wild-type RABA5c (upper panels) or RABA5c^{N125I} (lower panels) were observed at indicated times after flg22 treatment. Expression of RABA5c and RABA5c^{N125I} was induced by estradiol treatment. Bar = 5 μm.

(B) Stacked bar graphs indicating results of quantitative analyses of colocalization between FLS2-GFP and mRFP-SYP61. WT, wild-type RABA5c-expressing cells; NI, RABA5c^{N125I}-expressing cells. Data are collected from three independent experiments, and 206 and 156 (WT) or 208 and 143 (NI) FLS2-positive dots in total were observed in early (80–140) and late (140–200) stages, respectively. Error bars indicate SD values.

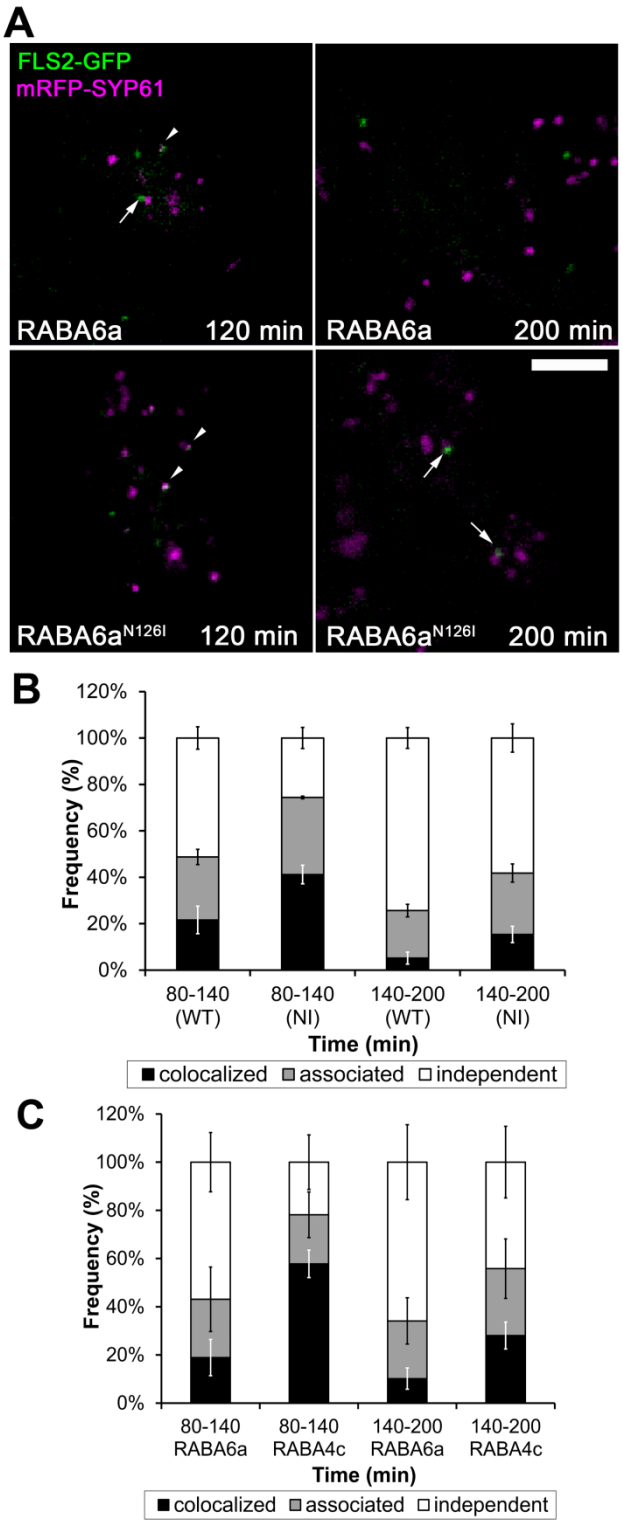

Figure 11. The NI mutant of RABA6a increases the ratio of compartments with both FLS2-GFP and mRFP-SYP61.

(A) Cells expressing FLS2-GFP and mRFP-SYP61 with wild-type RABA6a (upper

panels) or RABA6a^{N126I} (lower panels) were observed after 120 min or 200 min after flg22 treatment. Expression of RABA6a and RABA6a^{N126I} was induced by estradiol treatment. Arrowheads and arrows indicate FLS2-GFP signals colocalized and associated with TagRFP-SYP61, respectively. Bar = 5 μm.

(**B**) Stacked bar graphs indicating results of quantitative analyses of colocalization between FLS2-GFP and mRFP-SYP61. WT, wild-type RABA6a-expressing cell; NI, RABA6a^{N126I}-expressing cells. Data were collected from three independent experiments, and 178 and 162 (WT) or 204 and 209 (NI) FLS2-positive dots in total were observed in early (80–140) and late (140–200) stages, respectively. Error bars indicate SD values.

(**C**) Stacked bar graphs indicating results of quantitative analyses of colocalization between FLS2-GFP and CFP-SYP61 in RABA6a^{N126I}-expressing cells. RABA6a, RABA6a-coexpressing cell; RABA4c, RABA4c-coexpressing cells. Data were collected from three independent experiments, 64 and 51 (RABA6a) or 118 and 87 (RABA4c) FLS2-positive dots in total were observed in early (80–140) and late (140–200) stages, respectively. Error bars indicate SD values.

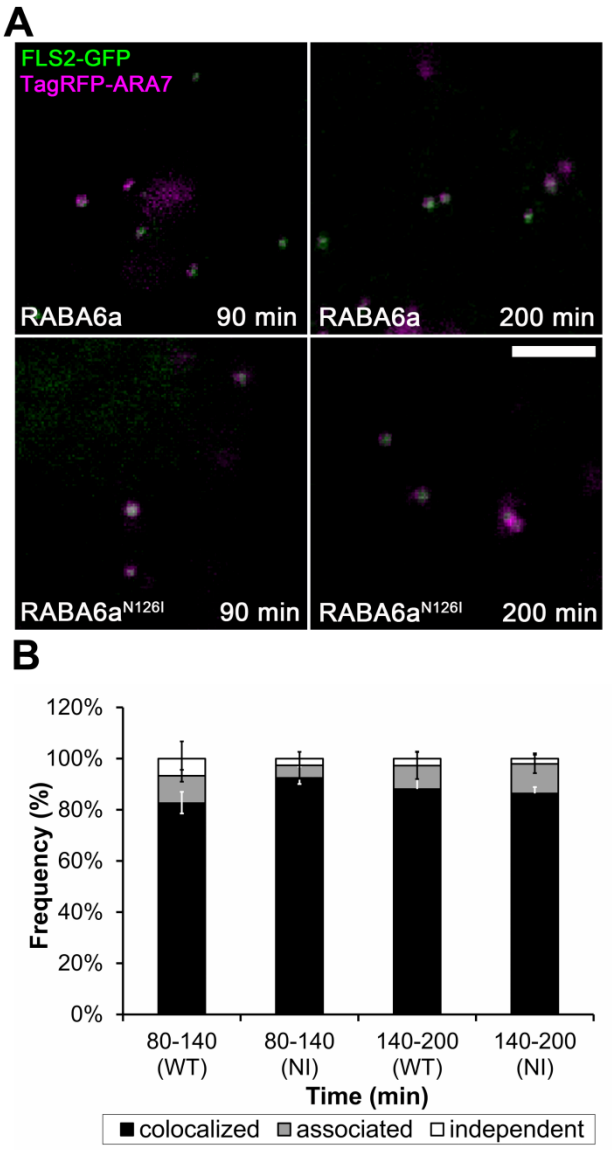

Figure 12. The NI mutant of RABA6a does not affect trafficking kinetics of FLS2-GFP to TagRFP-ARA7.

(**A**) Colocalization between FLS2-GFP and TagRFP-ARA7 in RABA6a^{N126I}-expressing cells. Endocytosed FLS2-GFP and TagRFP-ARA7 colocalized in both RABA6a- (upper panel) and RABA6a^{N126I}-expressing cells (bottom panel) after flg22 treatment. Bar = 5 μm.

(**B**) Stacked bar graphs indicating results of quantitative analyses of colocalization between FLS2-GFP and TagRFP-ARA7. WT, wild-type RABA6a-expressing cells; NI, RABA6a^{N126I}-expressing cells. Data are collected from three independent experiments, and 295 and 162 (WT) or 229 and 136 (NI) FLS2-positive dots in total were observed in early (80–140) and late (140–200) stages, respectively. Error bars indicate SD values.

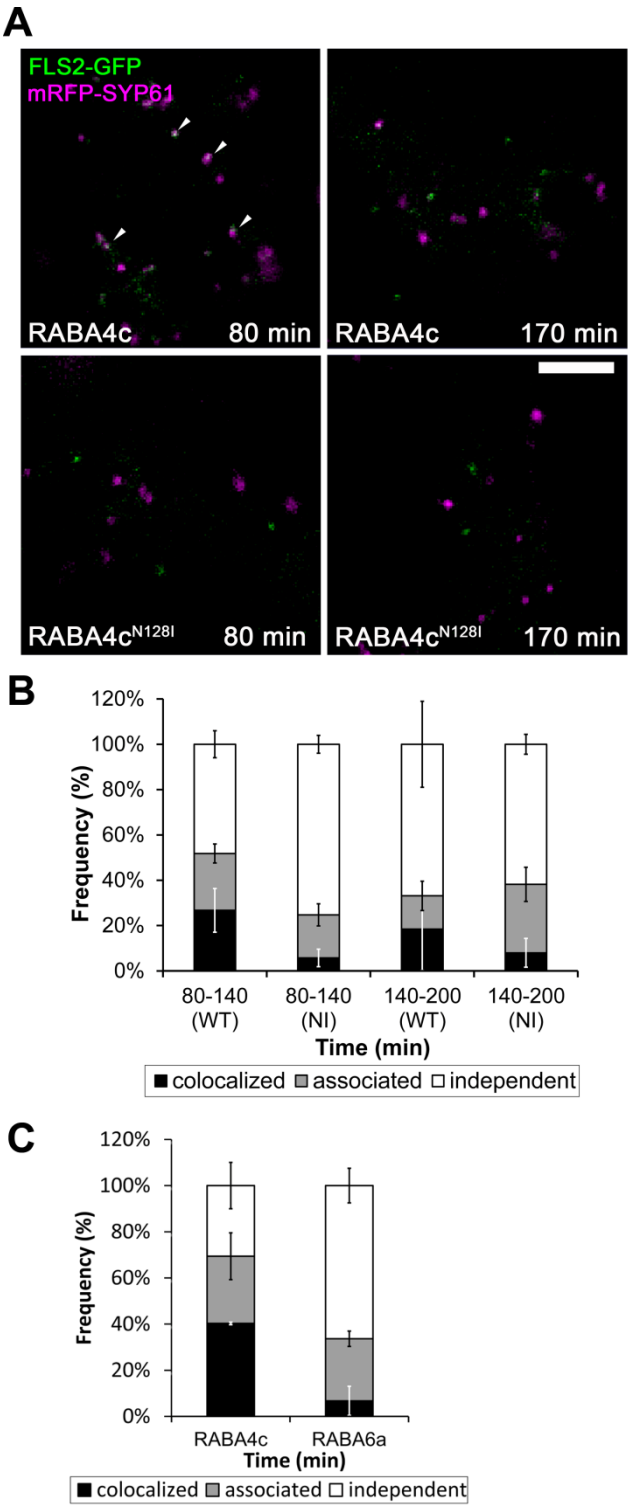

Figure 13. The NI mutant of RABA4c decreases the ratio of compartments with both FLS2-GFP and mRFP-SYP61.

(**A**) Cells expressing FLS2-GFP and mRFP-SYP61 with wild-type RABA4c (upper panels) or RABA4c^{N128I} (lower panels) were observed after 80 min or 170 min after flg22

treatment. Expression of RABA4c and RABA4c^{N128I} was induced by estradiol treatment. Arrowheads indicate FLS2-GFP signals colocalized with TagRFP-SYP61. Bar = 5 μm. Note that colocalization was not observed in RABA4c^{N128I}-expressing cells.

(**B**) Stacked bar graphs indicating results of quantitative analyses of colocalization between FLS2-GFP and mRFP-SYP61. WT, wild-type RABA4c-expressing cell; NI, RABA4c^{N128I}-expressing cells. Data were collected from three independent experiments, and 174 and 153 (WT) or 143 and 82 (NI) FLS2-positive dots in total were observed in early (80–140) and late (140–200) stages, respectively. Error bars indicate SD values.

(**C**) Stacked bar graphs indicating results of quantitative analyses of colocalization between FLS2-GFP and CFP-SYP61 in RABA4c^{N128I}-expressing cells. RABA4c, RABA4c-coexpressing cell; RABA6a, RABA6a-coexpressing cells. Data were collected from three independent experiments, 32 (RABA4c) or 30 (RABA6a) FLS2-positive dots in total were observed in the early (80–140) stage. Error bars indicate SD values.

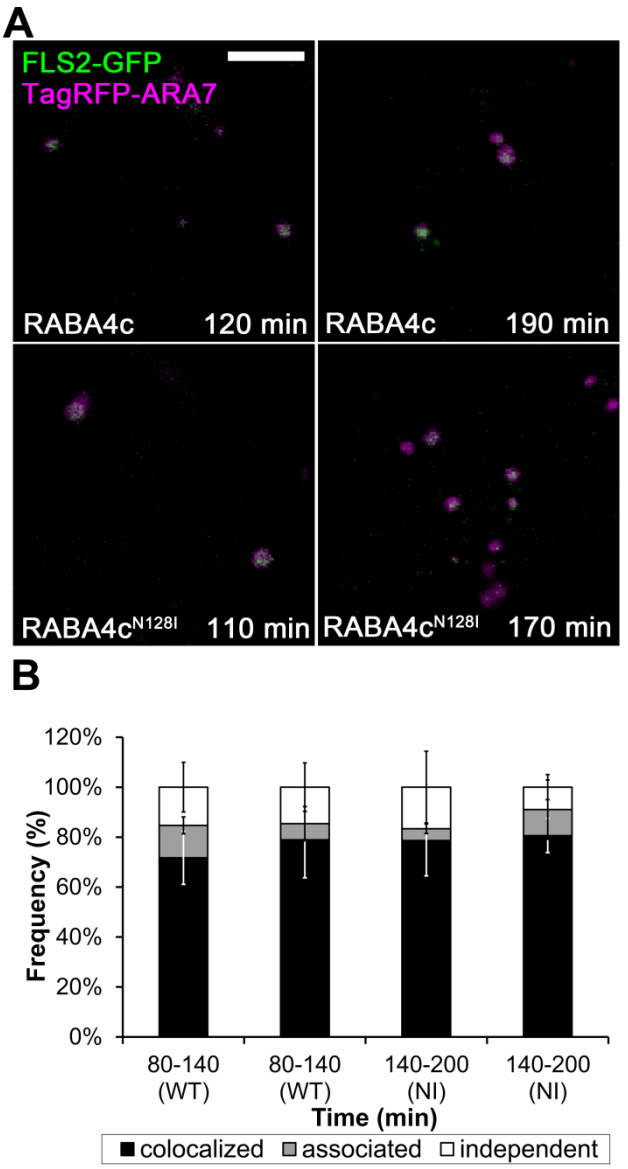

Figure 14. The NI mutant of RABA6a does not affect trafficking kinetics of FLS2-GFP to TagRFP-ARA7.

(A) FLS2-GFP and TagRFP-ARA7 colocalize in RABA4c- (upper panel) and RABA4c^{N126I}-expressing cells (bottom panel) after flg22 treatment. Bar = 5 μm.

(B) Stacked bar graphs indicating results of quantitative analyses of colocalization between FLS2-GFP and TagRFP-ARA7. WT, wild-type RABA4c-expressing cells; NI, RABA4c^{N128I}-expressing cells. Data are collected from three independent experiments, and 131 and 203 (WT) or 152 and 114 (NI) FLS2-positive dots in total were observed in early (80–140) and late (140–200) stages, respectively. Error bars indicate SD values.

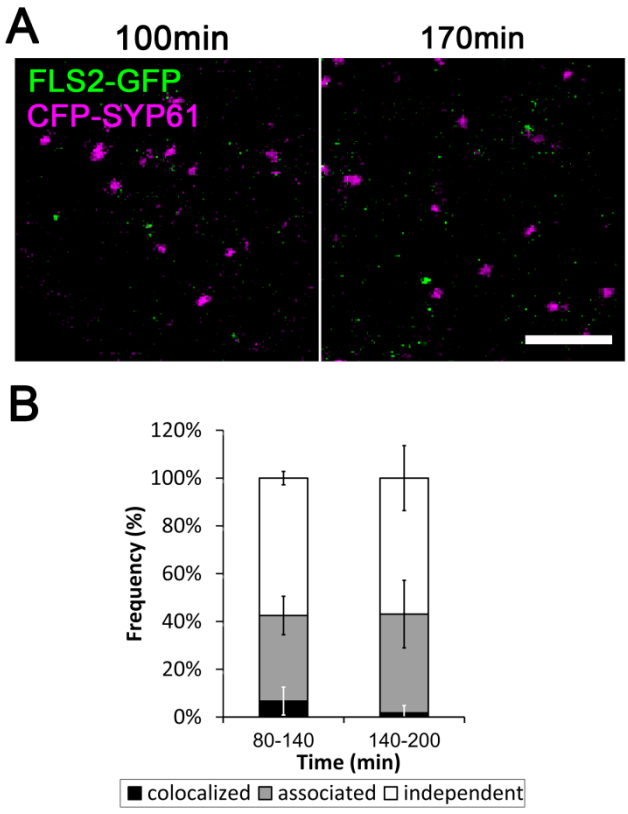

Figure 15. Coexpression of NI mutants of RABA4c and RABA6a.

(**A**) Cells expressing FLS2-GFP and CFP-SYP61 with both RABA6a^{N126I} and RABA4c^{N128I} were observed after 100 min or 170 min after flg22 treatment. Expression of RABA6a^{N126I} and RABA4c^{N128I} was induced by estradiol treatment. Bar = 5 μm. Note that colocalization was not observed in cells expressing RABA6a^{N126I} and RABA4c^{N128I}.

(**B**) Stacked bar graphs indicating results of quantitative analyses of colocalization between FLS2-GFP and CFP-SYP61. Data were collected from three independent experiments, 69 and 63 FLS2-positive dots in total were observed in early (80–140) and late (140–200) stages, respectively. Error bars indicate SD values.

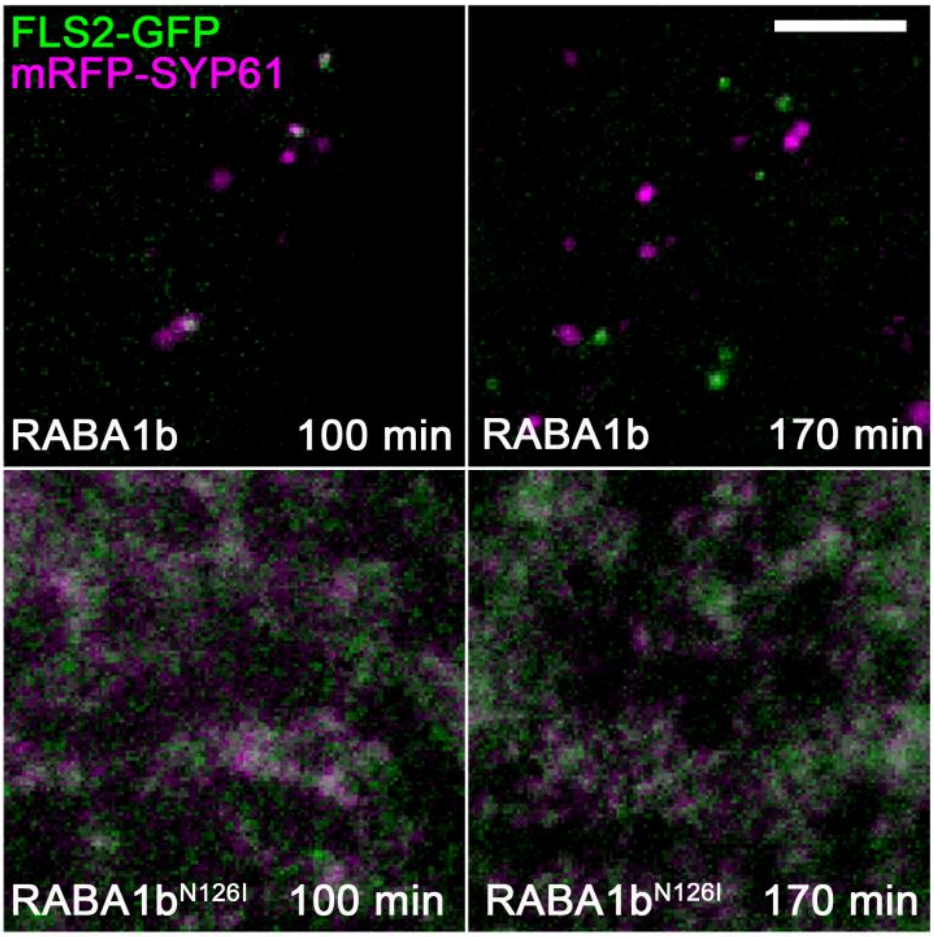

Figure 16. The NI mutant of RABA1b affects the localization pattern of mRFP-SYP61. Localization of FLS2-GFP and mRFP-SYP61 was observed at the indicated times after flg22 treatment in RABA1b- (upper panels) or RABA1b^{N126I}-expressing cells (lower panels). Expression of RABA1b and RABA1b^{N126I} was induced by estradiol treatment.

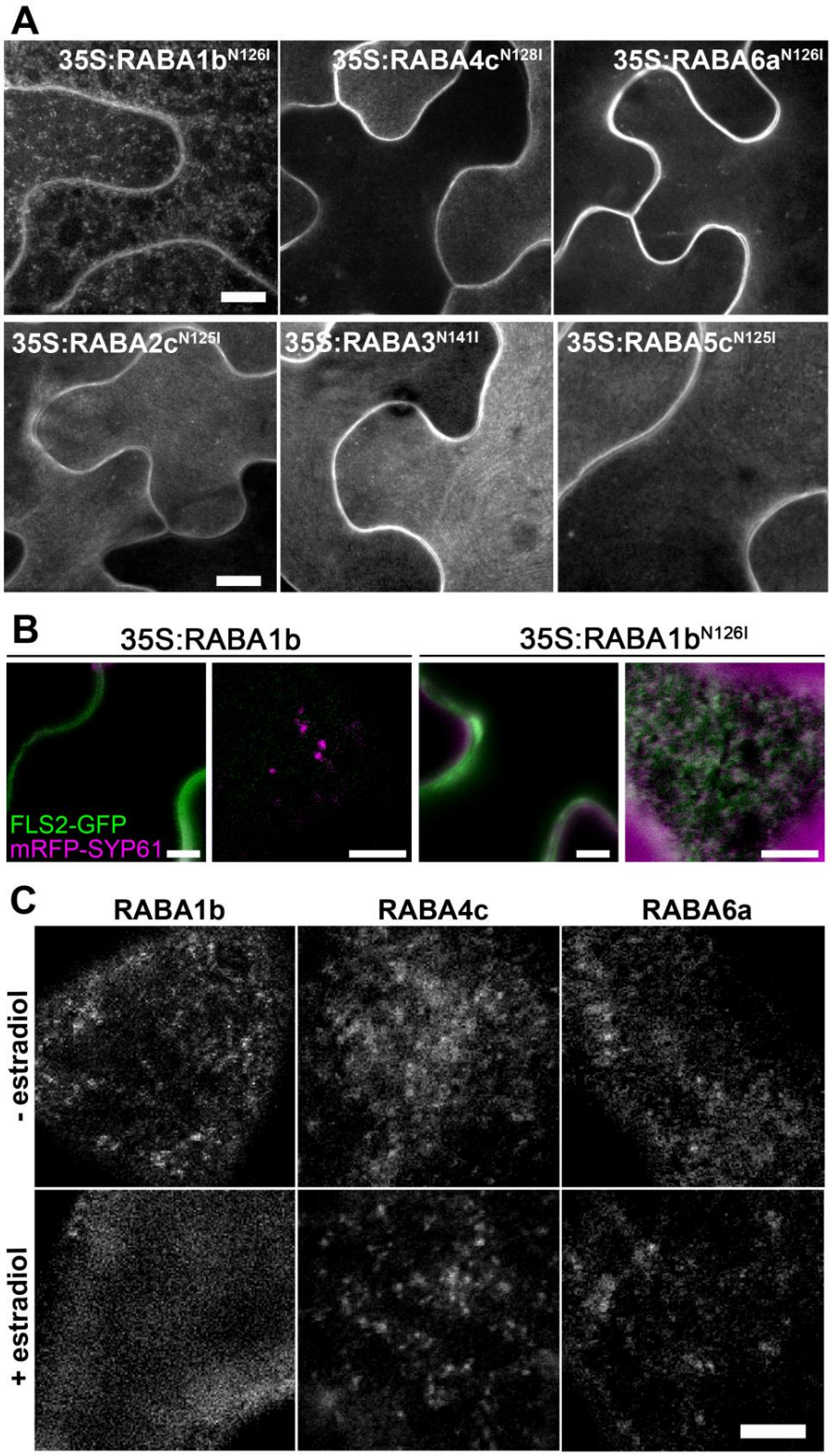

Figure 17. Constitutive expression of RABA1b^{N126I} alters steady-state localization of FLS2-GFP and mRFP-SYP61.

(A) Localization of FLS2-GFP in cells expressing RABA1b^{N126I} (left upper panel), RABA4c^{N128I} (middle upper panel), RABA6a^{N126I} (right upper panel), RABA2c^{N125I} (left lower panel), RABA3^{N141I} (middle lower panel), or RABA5c^{N125I} (right lower panel) under regulation of the 35S promoter. Max intensity projection images are presented, each of which is reconstructed with a series of confocal Z-stack images taken at 0.5-μm intervals. Bar = 5 μm.

(B) Localization of FLS2-GFP and mRFP-SYP61 in RABA1b- or RABA1b^{N126I}-expressing cells under regulation of the 35S promoter. Left panels show the middle plane of cells, and right panels show the confocal plane near the plasma membrane in the same cells shown in left panels. Bars = 5 μm.

(C) Localization of FLS2-GFP in cells expressing 35S promoter-drived RABA1b^{N126I} and estradiol-inducible promoter-drived RABA1b (left panel), RABA4c (middle panel), or RABA6a (right panel). Upper and lower panels indicate cells before and after estradiol treatment, respectively. Bar = 5 μm.

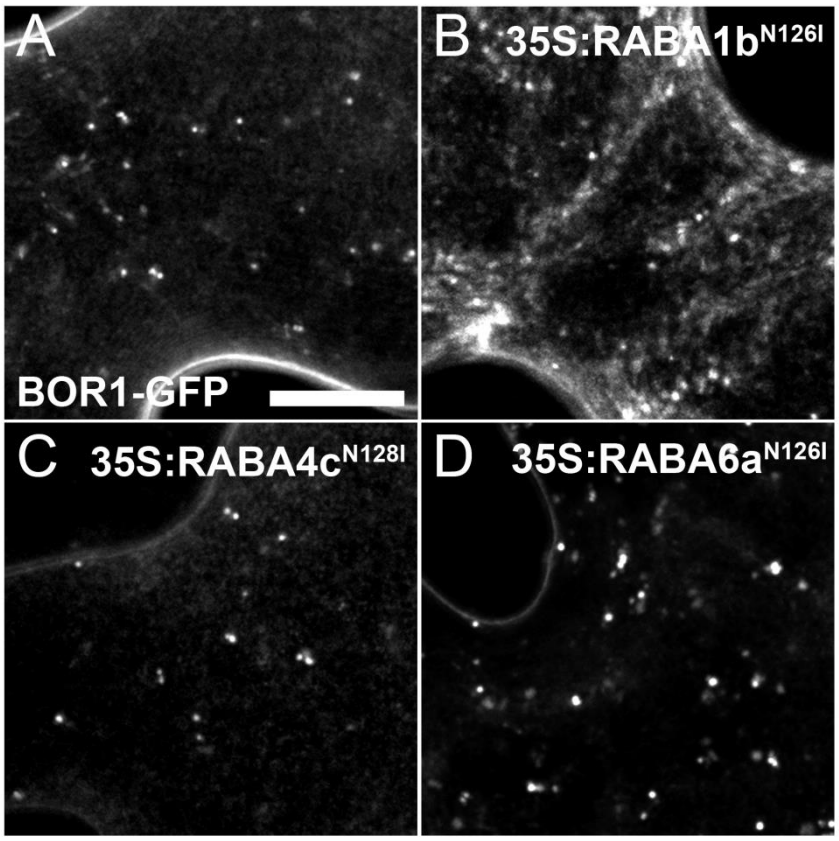

Figure 18. Constitutive expression of RABA1b^{N126I} alters steady-state localization of BOR1-GFP.

(**A**) Localization of BOR1-GFP.

(**B**) to (**D**) RABA1b^{N126I} (B), RABA4c^{N128I} (C), or RABA6a^{N126I} (D) were coexpressed under regulation of the 35S promoter in cells expressing BOR1-GFP. Max intensity projection images are presented, each of which is reconstructed with a series of confocal Z-stack images taken at 0.5-μm intervals. Bar = 5 μm.

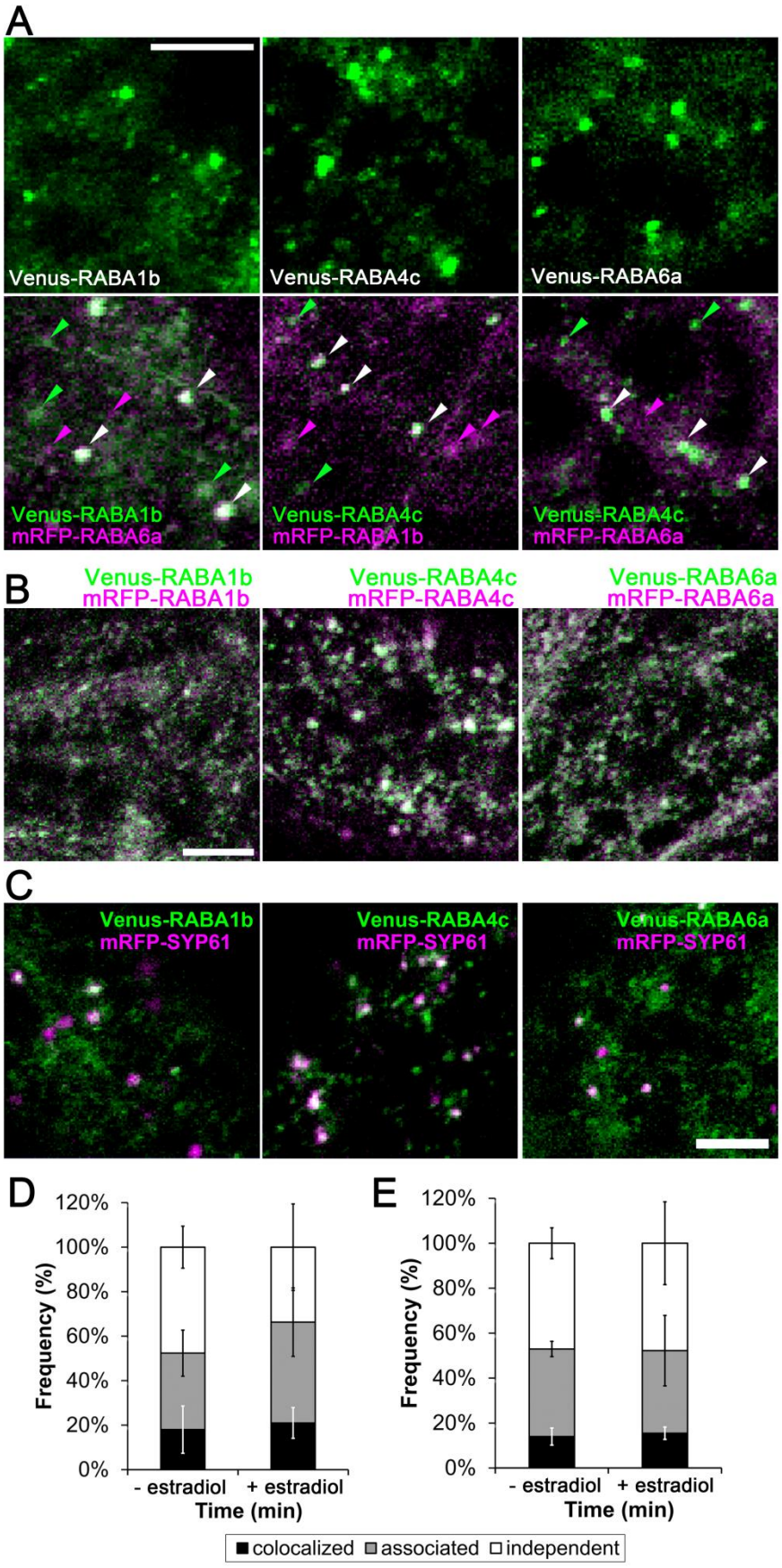
A
Venus-RABA1b
Venus-RABA4c
Venus-RABA6a
Venus-RABA1b
mRFP-RABA6a
Venus-RABA4c
mRFP-RABA1b
Venus-RABA4c
mRFP-RABA6a
B
Venus-RABA1b
mRFP-RABA1b
Venus-RABA4c
mRFP-RABA4c
Venus-RABA6a
mRFP-RABA6a
C
Venus-RABA1b
mRFP-SYP61
Venus-RABA4c
mRFP-SYP61
Venus-RABA6a
mRFP-SYP61
D
120%
100%
80%
60%
40%
20%
0%
Frequency (%)
- estradiol
+ estradiol
Time (min)
E
120%
100%
80%
60%
40%
20%
0%
Frequency (%)
- estradiol
+ estradiol
Time (min)
colocalized
associated
independent

Figure 19. Subcellular localization of RABA1b, RABA4c, and RABA6a

(**A**) All three RABA members localized on large clear punctate compartments and tiny scattering vesicles when expressed in *N. benthamiana* cells separately (upper panels). When two RABA members tagged with indicated fluorescent proteins were expressed in the same cells, they colocalized on the large compartments but not on the scattering vesicles (lower panels). Bar = 5 μm.

(**B**) When the same RABA members were tagged with different fluorescent proteins and expressed in the same cell, localization patterns overlapped almost completely. Bar = 5 μm.

(**C**) mRFP-SYP61 was coexpressed with RABA1b (left panel), RABA4c (middle panel), or RABA6a (right panel) in FLS2-GFP expressing cells. Bar = 5 μm.

(**D**) Stacked bar graphs indicating results of quantitative analyses of colocalization between CFP-SYP61 and mRFP-RABA1b in RABA4c^{N128I}. Data were collected from three independent experiments, and 282 and 269 SYP61-positive dots in total were observed in before and after treatment of estradiol to express RABA4c^{N128I}, respectively. Error bars indicate SD values.

(**E**) Stacked bar graphs indicating results of quantitative analyses of colocalization between CFP-SYP61 and mRFP-RABA1b in RABA6a^{N126I}. Data were collected from three independent experiments, and 116 and 97 SYP61-positive dots in total were observed in before and after treatment of estradiol to express RABA6a^{N126I}, respectively. Error bars indicate SD values.

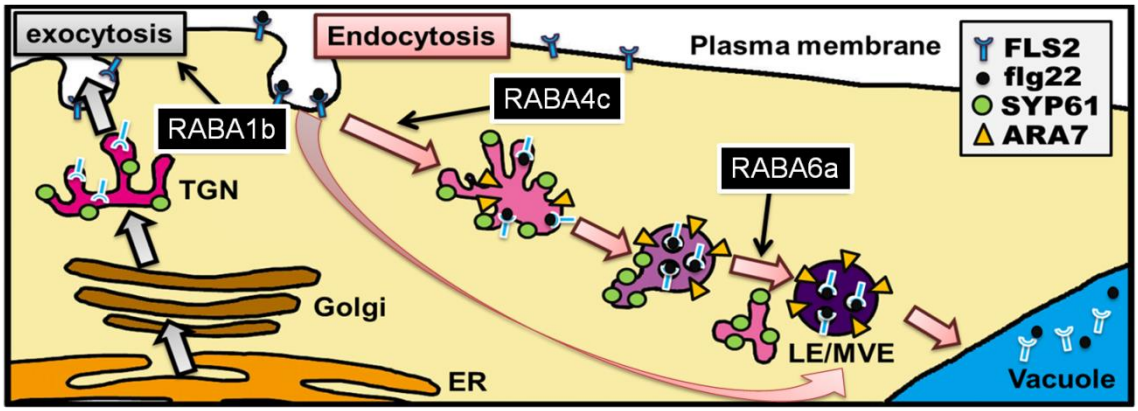

Figure 20. Schematic model of the function of RABA members on FLS2 trafficking route
On endocytic pathway, RABA4c regulates the process that internalized FLS2 by ligand recognition is transported to the intermediate endosomes which bear both feature of the TGN and MVE. RABA6a participates in the maturation step to MVE which only ARA7 localize on. On the other hand, RABA1b involves in exocytic pathway of FLS2 to the PM.

Tables

Table 1. Quantification of colocalization between SYP61 and ARA7

		Colocalized	Associated	Independent
+FLS2	No treat. (n = 335)	0.7% (± 0.6%)	21.0% (± 1.3%)	78.3% (± 0.7%)
	Early stage (n = 539)	4.6% (± 2.0%)	22.5% (± 2.2%)	72.9% (± 0.9%)
	Late stage (n = 470)	1.0% (± 0.9%)	19.8% (± 0.9%)	79.2% (± 1.1%)
-FLS2	No treat. (n = 536)	0.0% (± 0.0%)	22.0% (± 2.9%)	78.0% (± 2.9%)
	Early stage (n = 624)	1.1% (± 0.5%)	21.6% (± 1.8%)	77.3% (± 1.3%)
	Late stage (n = 532)	1.2% (± 1.0%)	20.0% (± 5.3%)	78.9% (± 5.5%)

SYP61-positive compartments were classified into three classes according to the criteria mentioned in the text in cells expressing FLS2-GFP (+FLS2) and cells that were not transformed with FLS2-GFP (-FLS2). Data were collected from three independent experiments.

Table 2. A List of RABA members

Groups	Members (Accession number)
RABA1	RABA1a (At1g06400), RABA1b (At1g16920), RABA1c (At5g45750), RABA1d (At4g18800), RABA1e (At4g18430), RABA1f (At5g60860), RABA1g (At3g15060), RABA1h (At2g33870), RABA1i (At1g28550)
RABA2	RABA2a (At1g09630), RABA2b (At1g07410), RABA2c (At3g46830), RABA2d (At5g59150)
RABA3	RABA3 (At1g01200)
RABA4	RABA4a (At5g65270), RABA4b (At4g39990), RABA4c (At5g47960), RABA4d (At3g12160), RABA4e (At2g22390)
RABA5	RABA5a (At5g47520), RABA5b (At3g07410), RABA5c (At2g43130), RABA5d (At2g31680), RABA5e (At1g05810)
RABA6	RABA6a (At1g73640), RABA6b (At1g18200)

All 26 members of RABA are classified into 6 groups. The members which I have tested are underlined.

References

Asaoka, R., Uemura, T., Ito, J., Fujimoto, M., Ito, E., Ueda, T., and Nakano, A. (2012). Arabidopsis RABA1 GTPases are involved in the transport between the trans-Golgi network and the plasma membrane and are required for salinity stress tolerance. Plant J. PMID: 22974509

Batoko, H., Zheng, H. Q., Hawes, C., and Moore, I. (2000). A rab1 GTPase is required for transport between the endoplasmic reticulum and golgi apparatus and for normal golgi movement in plants. Plant Cell **12**: 2201-18.

Beck, M. Zhou, J., Faulkner, C., Maclean, D., and Robatzek, S. (2012). Spatio-Temporal Cellular Dynamics of the Arabidopsis Flagellin Receptor Reveal Activation Status-Dependent Endosomal Sorting. Plant Cell **24**: 4205-19.

Benli, M., Döring, F., Robinson, D. G., Yang, X., and Gallwitz, D. (1996). Two GTPase isoforms, Ypt31p and Ypt32p, are essential for Golgi function in yeast. EMBO J. **15**: 6460-75.

Bolte, S., Brown, S., and Satiat-Jeunemaitre, B. (2004). The N-myristoylated Rab-GTPase m-Rabmc is involved in post-Golgi trafficking events to the lytic vacuole in plant cells. J Cell Sci. **117**: 943-54.

Bottanelli, F., Foresti, O., Hanton, S., and Denecke, J. (2011). Vacuolar Transport in Tobacco Leaf Epidermis Cells Involves a Single Route for Soluble Cargo and Multiple Routes for Membrane Cargo. Plant Cell **23**: 3007-3025.

Boutté, Y., Frescatada-Rosa, M., Men, S., Chow, C.M., Ebine, K., Gustavsson, A., Johansson, L., Ueda, T., Moore, I., Jürgens, G., and Grebe, M.. (2010). Endocytosis restricts Arabidopsis KNOLLE syntaxin to the cell division plane during late cytokinesis. EMBO J. **29**: 546–58.

Cheng, H., Sugiura, R., Wu, W., Fujita, M., Lu, Y., Sio, S. O., Kawai, R., Takegawa, K., Shuntoh H., and Kuno T. (2002). Role of the Rab GTP-Binding Protein Ypt3 in the Fission Yeast Exocytic Pathway and Its Connection to Calcineurin Function. Mol Biol Cell. **13**: 2963-2976.

Cheung A. Y., Chen C. Y., Glaven R. H., de Graaf B. H., Vidali L., Hepler P.K., and Wu H.M. (2002). Rab2 GTPase regulates vesicle trafficking between the endoplasmic reticulum and the Golgi bodies and is important to pollen tube growth. Plant Cell **14**: 945-962.

Chow, C. M., Neto, H., Foucart, C., and Moore, I. (2008). Rab-A2 and Rab-A3 GTPases define a trans-golgi endosomal membrane domain in Arabidopsis that contributes substantially to the cell plate. Plant Cell **20**: 101-23.

Curtis, M. D., and Grossniklaus, U. (2003). A Gateway Cloning Vector Set for High-Throughput Functional Analysis of Genes in Planta. Plant Physiol. **133**: 462-469.

Dettmer, J., Hong-hermesdorf, A., Stierhof, Y.-dieter, and Schumacher, K. (2006). Vacuolar H 1 -ATPase Activity Is Required for Endocytic and Secretory Trafficking in Arabidopsis. Plant Cell **18**: 715-730.

de Graaf, B. H. J., Cheung, A., and Andreyeva, T. (2005). Rab11 GTPase-regulated membrane trafficking is crucial for tip-focused pollen tube growth in tobacco. Plant Cell **17**: 2564-2579.

Ebine, K., Fujimoto, M., Okatani, Y., Nishiyama, T., Goh, T., Ito, E., Dainobu, T., Nishitani A., Uemura T., Sato M.H., Thordal-Christensen H., Tsutsumi N., Nakano A., and Ueda T. (2011). A membrane trafficking pathway regulated by the plant-specific RAB GTPase ARA6. Nat Cell Biol. **13**: 853-9.

Ebine, K., Okatani, Y., Uemura, T., Goh, T., Shoda, K., Niihama, M., Morita, M. T., Spitzer C., Otegui M.S., Nakano A., and Ueda T. (2008). A SNARE complex unique to seed plants is required for protein storage vacuole biogenesis and seed development of Arabidopsis thaliana. Plant Cell **20**: 3006-21.

Feraru, E., Feraru, M.I., Asaoka, R., Paciorek, T., De Rycke, R., Tanaka, H., Nakano, A., and Friml, J. (2012). BEX5/RabA1b regulates trans-golgi network-to-plasma membrane protein trafficking in Arabidopsis. Plant Cell **24**: 3074–86.

Fujimoto, M., Arimura, S., Nakazono, M., and Tsutsumi, N. (2007). Imaging of plant dynamin-related proteins and clathrin around the plasma membrane by variable incidence angle fluorescence microscopy. Plant Biotech. **24**: 449–455.

Geldner, N., Hyman, D. L., Wang, X., Schumacher, K., and Chory, J. (2007). Endosomal signaling of plant steroid receptor kinase BRI1. Genes Dev. **21**: 1598-602.

Gendre, D., Oh, J., Boutté, Y., Best, J.G., Samuels, L., Nilsson, R., Uemura, T., Marchant, A., Bennett, M.J., Grebe, M., and Bhalerao, R.P. (2011). Conserved Arabidopsis ECHIDNA protein mediates trans-Golgi-network trafficking and cell elongation. Proc Natl Acad Sci U S A. **108**: 8048–53.

Goodin, M.M., Chakrabarty, R., Yelton, S., Martin, K., Clark, A., and Brooks, R. (2007a). Membrane and protein dynamics in live plant nuclei infected with Sonchus yellow net virus, a plant-adapted rhabdovirus. J Gen Virol. **88**: 1810–20.

Goodin, M.M., Chakrabarty, R., Banerjee, R., Yelton, S., and Debolt, S. (2007b). New gateways to discovery. Plant Physiol. **145**: 1100–9.

Irani N.G., Di Rubbo S., Mylle E., Van den Begin J., Schneider-Pizoń J., Hniliková J., Síša M., Buyst D., Vilarrasa-Blasi J., Szatmári A.M., Van Damme D., Mishev K., Codreanu M.C., Kohout L., Strnad M., Caño-Delgado A.I., Friml J., Madder A., Russinova E. (2012). Fluorescent castasterone reveals BRI1 signaling from the plasma membrane. Nat Chem Biol. **8**: 583-9.

Ito, E., Fujimoto, M., Ebine, K., Uemura, T., Ueda, T., and Nakano, A. (2011). Dynamic behavior of clathrin in Arabidopsis thaliana unveiled by live imaging. Plant J. **69**: 204-216.

Jedd, G., Mulholland, J., and Segev, N. (1997). Two New Ypt GTPases Are Required for Exit From the Yeast. Cell. **137**: 563-580.

Karimi, M., Inzé, D., and Depicker, A. (2002). GATEWAY vectors for Agrobacterium-mediated plant transformation. Trends Plant Sci. **7**: 193-195.

Konopka, C., and Bednarek, S.Y. (2008). Comparison of the dynamics and functional redundancy of the Arabidopsis dynamin-related isoforms DRP1A and DRP1C during plant development. Plant Physiol. **147**: 1590–602.

Kotzer, A. M., Brandizzi, F., Neumann, U., Paris, N., Moore, I., and Hawes, C. (2004). AtRabF2b (Ara7) acts on the vacuolar trafficking pathway in tobacco leaf epidermal cells. J Cell Sci. **117**: 6377-89.

Lam, S. K., Siu, C. L., Hillmer, S., Jang, S., An, G., Robinson, D. G., and Jiang, L. (2007). Rice SCAMP1 defines clathrin-coated, trans-golgi-located tubular-vesicular structures as an early endosome in tobacco BY-2 cells. Plant Cell **19**: 296-319.

Li, R., Liu, P., Wan, Y., Chen, T., Wang, Q., Mettbach, U., Baluska, F., Samaj J., Fang X., Lucas W.J., and Lin J. (2012). A Membrane Microdomain-Associated Protein, Arabidopsis Flot1, Is Involved in a Clathrin-Independent Endocytic Pathway and Is Required for Seedling Development. Plant Cell **24**:2105-22.

Martin, K., Kopperud, K., Chakrabarty, R., Banerjee, R., Brooks, R., and Goodin, M.M. (2009). Transient expression in Nicotiana benthamiana fluorescent marker lines provides enhanced definition of protein localization, movement and interactions in planta. Plant J. **59**: 150–162.

Nakagawa, T., Kurose, T., Hino, T., Tanaka, K., Kawamukai, M., Niwa, Y., Toyooka, K., Matsuoka K., Jinbo T., and Kimura T. (2007). Development of series of gateway binary vectors, pGWBs, for realizing efficient construction of fusion genes for plant transformation. J Biosci Bioeng. **104**: 34-41.

Platta, H. W., and Stenmark, H. (2011). Endocytosis and signaling. Curr Opin Cell Biol. **23**: 393-403.

Preuss, M. L., Serna, J., Falbel, T. G., Bednarek, S. Y., and Nielsen, E. (2004). The Arabidopsis Rab GTPase RabA4b Localizes to the Tips of Growing Root Hair Cells. Plant Cell **16**: 1589-1603.

Ren, M., Xu, G., Zeng, J., De Lemos-Chiarandini, C., Adesnik, M., and Sabatini, D. D. (1998). Hydrolysis of GTP on rab11 is required for the direct delivery of

transferrin from the pericentriolar recycling compartment to the cell surface but not from sorting endosomes. Proc. Natl. Acad. Sci. USA **95**: 6187-92.

Rink, J., Ghigo, E., Kalaidzidis, Y., and Zerial, M. (2005). Rab conversion as a mechanism of progression from early to late endosomes. Cell **122**: 735-49.

Robatzek, S., Chinchilla, D., and Boller, T. (2006). Ligand-induced endocytosis of the pattern recognition receptor FLS2 in Arabidopsis. Genes Dev. **20**: 537-42.

Rutherford, S., and Moore, I. (2002). The Arabidopsis Rab GTPase family: another enigma variation. Curr Opin Plant Biol. **5**: 518-528.

Scheuring, D., Viotti, C., Krüger, F., Künzl, F., Sturm, S., Bubeck, J., Hillmer, S., Frigerio L., Robinson D.G., Pimpl P., and Schumacher K. (2011). Multivesicular Bodies Mature from the Trans-Golgi Network/Early Endosome in Arabidopsis. Plant Cell **23**: 3463-3481.

Sohn E.J., Kim E.S., Zhao M., Kim S.J., Kim H., Kim Y.W., Lee Y.J., Hillmer S., Sohn U., Jiang L., and Hwang I. (2003). Rha1, an Arabidopsis Rab5 Homolog, Plays a Critical Role in the Vacuolar Trafficking of Soluble Cargo Proteins. Plant Cell **15**: 1057-70.

Sorkin, A., and Von Zastrow, M. (2002). Signal transduction and endocytosis: close encounters of many kinds. Nat Rev Mol Cell Biol. **3**: 600-14.

Stierhof, Y. D., and El Kasmi, F. (2010). Strategies to improve the antigenicity, ultrastructure preservation and visibility of trafficking compartments in Arabidopsis tissue. Eur J Cell Biol. **89**: 285-97.

Szumlanski, A. L., and Nielsen, E. (2009). The Rab GTPase RabA4d regulates pollen tube tip growth in Arabidopsis thaliana. Plant Cell **21**: 526-44.

Takano, J., Miwa, K., Yuan, L., von Wirén, N., and Fujiwara, T. (2005). Endocytosis and degradation of BOR1, a boron transporter of Arabidopsis thaliana, regulated by boron availability. Proc. Natl. Acad. Sci. USA **102**: 12276-81.

Takano, J., Noguchi, K., Yasumori, M., Kobayashi, M., Gajdos, Z., Miwa, K., Hayashi, H., Yoneyama T., and Fujiwara T. (2002). Arabidopsis boron transporter for xylem loading. Nature **420**: 337-40.

Tardif, G., Kane, N.A., Adam, H., Labrie, L., Major, G., Gulick, P., Sarhan, F., and Laliberté, J.F. (2007). Interaction network of proteins associated with abiotic stress response and development in wheat. Plant Mol Biol. **63**: 703–18.

Ueda, T., Yamaguchi, M., Uchimiya, H., and Nakano, A. (2001). Ara6, a plant-unique novel type Rab GTPase, functions in the endocytic pathway of Arabidopsis thaliana. EMBO J **20**: 4730-41.

Uemura, T. Kim, H., Saito, C., Ebine, K., Ueda, T., Schulze-Lefert, P., and Nakano A. (2012). Qa-SNAREs localized to the trans-Golgi network regulate multiple transport pathways and extracellular disease resistance in plants. Proc. Natl. Acad. Sci. USA **109**: 1784-9

Uemura, T., Ueda, T., Ohniwa, R. L., Nakano, A., Takeyasu, K., Sato, M. H. (2004). Systematic analysis of SNARE molecules in Arabidopsis: dissection of the post-Golgi network in plant cells. Cell Struct Funct. **29**: 49-65.

Ullrich, O. (1996). Rab11 regulates recycling through the pericentriolar recycling endosome. J Cell Biol. **135**: 913-924.

Vernoud, V., Horton, A. C., Yang, Z., and Nielsen, E. (2003). Analysis of the Small GTPase Gene Superfamily of Arabidopsis. Plant Physiol. **131**: 1191-1208.

Viotti, C., Bubeck, J., Stierhof, Y.D., Krebs, M., Langhans, M., van den Berg, W., van Dongen, W., Richter S., Geldner N., Takano J., Jürgens G., de Vries S.C., Robinson D.G., and Schumacher K. (2010). Endocytic and Secretory Traffic in Arabidopsis Merge in the Trans-Golgi Network/Early Endosome, an Independent and Highly Dynamic Organelle. Plant Cell **22**: 1344-57.

Voinnet, O., Rivas, S., Mestre, P., and Baulcombe, D. (2003). An enhanced transient expression system in plants based on suppres- sion of gene silencing by the p19 protein of tomato bushy stunt virus. Plant J. 33: 949–956.

von Zastrow, M., and Sorkin, A. (2007). Signaling on the endocytic pathway. Curr Opin Cell Biol. **19**: 436-45.

Wang, F., Liu, C., Wei, C., Cui, Y., Zheng, Q., Zhang, J., Wu, J., et al., and Liu, K. (2011). AtRabD2b, a Functional Ortholog of the Yeast Ypt1, Controls Various Growth and Developmental Processes in Arabidopsis. Plant Mol Biol Rep. **30**: 275-285.

Zipfel, C., Robatzek, S., Navarro, L., Oakeley, E. J., Jones, J. D. G., Felix, G., and Boller, T. (2004). Bacterial disease resistance in Arabidopsis through flagellin perception. Nature **428**: 764-7.

Zuo, J., Niu, Q.-W., and Chua, N.-H. (2000). An estrogen receptor-based transactivator XVE mediates highly inducible gene expression in transgenic plants. Plant J. **24**: 265-273.